CHALMERS

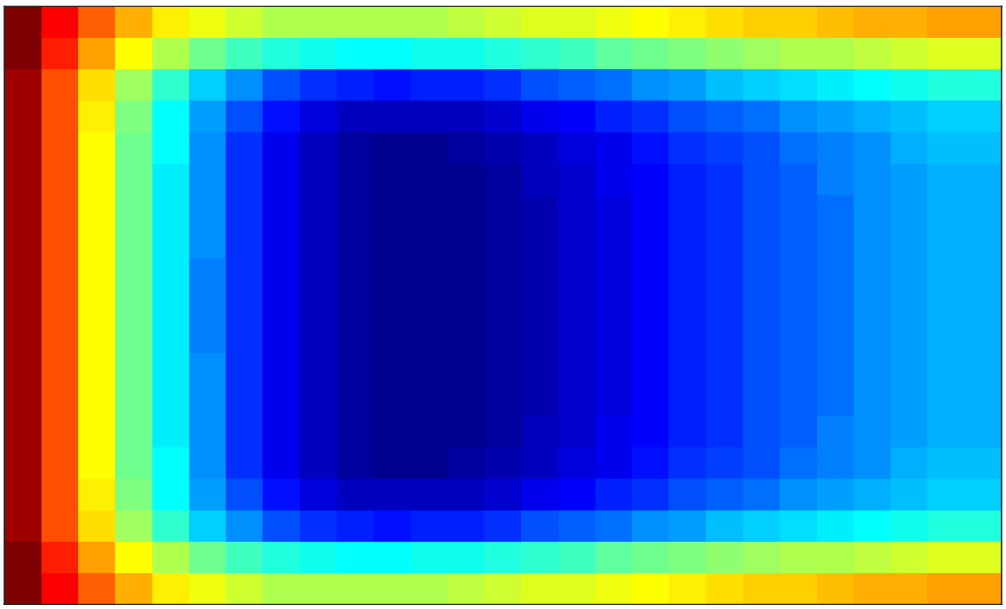

Modelling of a Purge Heated Carbon Canister Using CFD

Master's Thesis in Innovative and Sustainable Chemical Engineering

ERIK ÖSTERMARK

Department of Chemistry and Chemical Engineering
CHALMERS UNIVERSITY OF TECHNOLOGY
Gothenburg, Sweden 2018

THESIS FOR THE DEGREE OF MASTER OF SCIENCE

Modelling of a Purge Heated Carbon Canister Using CFD

ERIK ÖSTERMARK

Chemical Engineering
Department of Chemistry and Chemical Engineering
CHALMERS UNIVERSITY OF TECHNOLOGY
Gothenburg, Sweden 2018

Modelling of a Purge Heated Carbon Canister Using CFD
ERIK ÖSTERMARK

Carried out for Volvo Cars
Supervisors at Volvo Cars: Robert Johansson & Göran Fredriksson
Examiner at Chalmers: Derek Creaser

Chemical Engineering
Department of Chemistry and Chemical Engineering
Chalmers University of Technology
SE-412 96 Gothenburg
Sweden
Telephone: +46 (0) 31 772 1000

Front cover illustration:
A contour plot of temperature in a carbon bed during purging of an experimental carbon canister.

Abstract

Volatile organic compounds found in motor vehicle fuel vapours are hazardous to human health and to the environment, and their release from vehicles to the environment must be controlled. Activated carbon canisters are used in petrol-driven vehicles to prevent the release of fuel vapours, by having them adsorb on a bed of activated carbon and subsequently desorbing (purging) them from the carbon using a flow of fresh air leading to the combustion engine. In this study, a simulation model of an activated carbon canister was developed featuring heating of the purge flow and two-dimensional heat transfer.

The Linear Driving Force model and the Dubinin-Astakhov adsorption isotherm were used to describe the equilibrium and rate of adsorption. These were incorporated into a CFD model in GT-SUITE to simulate the flow, heat and mass transfer in a simplified canister geometry. An experimental canister was built and used in adsorption and desorption experiments to provide data with which the model was calibrated and validated.

The resulting calibrated model shows a varying degree of accuracy compared to experimental data. Modelling of fuel vapour release from the carbon is accurate, while the modelling of temperature effects in the canister is less accurate. The simulated cases of heating during the purge event shows results in agreement with the expected behaviour, but experimental data for validation of these results are unavailable.

The primary conclusion is that the experimental methods provide insufficient data for accurate calibration of the model. Additions to the methods are suggested to provide the necessary data. Furthermore, the efficiency of heat addition to increase the purge capacity is reduced as more heat is supplied, and the model can be used to investigate such effects in different heating configurations. The influence of modelling heat transfer in two dimensions grows more important as the canister diameter increases. For sufficiently small carbon bed diameters, CPU-costs can be reduced by modelling only in 1D.

Keywords: activated carbon canister, purge heating, heat transfer, GT-SUITE, Linear Driving Force, Dubinin-Astakhov, adsorption

Acknowledgements

I have had a lot of help with this thesis project from many people, for which I am grateful. First and foremost I want to thank my supervisors Robert Johansson, Göran Fredriksson and Ehsan Yasari at Volvo Cars for the continuous help, support and feedback they have provided me with. There are also numerous employees at Volvo Cars who have kindly taken the time to help me a lot with the experimental part of the project. The guys at the fine mechanics workshop who built my experimental canister deserve thanks, as well as Anders Aronsson, Rickard Magnusson, Krister Blom and Kjell Arby who all helped me get set up for my butane experiments. Thanks also to Christer Berg for taking the time to help me carry out the pressure drop experiments.

Huge thanks to Meisam Farzaneh at Volvo Cars and Jonathan Brown at Gamma Technologies for their efforts to help me get the two-dimensional simulations to work well. Thanks also to Timothy Byrne and Peter McCrae at Ingevity for the kind treatment of my data requests.

Thanks to my examiner Derek Creaser at Chalmers University of Technology for reading my report drafts and for providing insightful and valuable feedback on my questions and methods.

Thanks to all my friends and family that have supported and encouraged me throughout my studies.

Contents

List of Figures

List of Tables

List of Symbols

Latin Symbols

A	Antoine equation parameter	-
A_c	Cross sectional area	m^2
A_w	Wall surface area for heat transfer	m^2
B	Antoine equation parameter	-
C	Antoine equation parameter	-
C_s	Surface concentration in a particle	mol/m^3
$\bar{c}$	Average adsorbed species concentration in a solid particle	mol/m^3
$c_{p,f}$	Fluid phase specific heat capacity	J/kg,K
D_{eff}	Effective intraparticle diffusivity	m^2/s
D_{eq}	Equivalent diameter	m
D_p	Effective particle diameter	m
dx	Axial discretisation length of discrete volumes	m
E	Characteristic energy of adsorption	J/mol
E_r	Activation energy of a reaction	J/mol
f	Friction factor	-
f_f	Fanning friction factor	-
F_s	Solid fraction of a packed bed	-
ΔG_{ads}	Gibb's free energy change	J/mol
H	Specific enthalpy	J/kg

h	Interphase convective heat transfer coefficient	W/m^2,K
h_{ex}	External convective heat transfer coefficient	W/m^2,K
h_w	Fluid-to-wall convective heat transfer coefficient	W/m^2,K
ΔH_{ads}	Adsorption enthalpy	J/mol
$\Delta H_{R,k}$	Reaction enthalpy of reaction k	J/mol
j_H	Chilton-Colburn j-factor for heat transfer	-
k_L	Effective LDF mass transfer coefficient	1/s
K_p	Coefficient of pressure loss	-
L	Packed bed length	m
n	Dubinin-Astakhov adsorption parameter	-
N_{W-P}	Weisz-Prater parameter	-
p	Pressure	Pa
p_s	Saturation vapour pressure	Pa
q	Number of moles adsorbed per unit mass of adsorbent	mol/kg
q_{radial}	Radial heat flux	J/m^2,s
Q	Power source	J/s
R	Universal gas constant	J/mol,K
R_p	Particle radius	m
r_k	Rate of reaction with index k	mol/m^3,s
r_{obs}	Observed reaction rate	mol/m^3,s
ΔR_{radial}	Radial discretisation length	m
Re_b	Packed bed Reynolds number	-
S	Specific area of a packed bed	m^2/m^3
S_{ex}	Specific external area of a vessel	m^2/m^3
ΔS_{ads}	Entropy change due to adsorption	J/mol,K
T	Temperature	K

t	Time	s
T_{ex}	External temperature	K
T_f	Fluid temperature	K
T_s	Solid temperature	K
T_w	Wall temperature	K
$\Delta T_{s,radial}$	Solid temperature difference between radially adjacent discrete volumes	K
u	Fluid velocity	m/s
u_{is}	Interstitial fluid velocity	m/s
u_s	Superficial fluid velocity	m/s
v	Volume of gas	m^3
V	Volume of a discrete volume	m^3
V_m	Volume per mole of adsorbed species	m^3/mol
W	Mass of adsorbed species per unit volume of packed bed	g/L
W_0	Mass of adsorbed species per unit volume of packed bed at the saturation pressure (limiting pore volume)	g/L

Greek symbols

ϵ	Potential energy of adsorption	J/mol
ε_b	Packed bed void fraction	-
θ	Fractional coverage of adsorbed species	-
λ_f	Fluid phase thermal conductivity	W/m,K
λ_s	Solid phase thermal conductivity	W/m,K
Λ	Active site density	mol/m^3
μ	Fluid dynamic viscosity	$Pa \cdot s$
ρ	Fluid density	kg/m^3
$\sigma_{j,k}$	Stoichiometric coefficient of species j in reaction k	-
ϕ	Volume of adsorbed species enclosed by surface of equipotential energy	m^3/kg
Ψ	Effective heat capacity of a packed bed	J/m^3,K
$\Omega_{f,j}$	Fluid phase mass fraction	-

Chapter 1

Introduction

This chapter is intended to provide an introduction for the reader to the subject of evaporative emissions control, the activated carbon canister and the different factors that affect the performance of a canister-equipped evaporative emissions control system. In relation to this, the objectives, demarcations and methods of this thesis project are presented.

1.1 Problem introduction

1.1.1 Volatile organic compounds, environment and release

The fuel in petrol-driven cars consists of a variety of different hydrocarbons of varying volatility. The evaporation of the fuel constitutes a source of what is generally referred to as volatile organic compound (VOC) emissions. This group of compounds can be loosely defined as gaseous carbon-containing compounds that exist in the atmosphere, not including elemental carbon, carbon monoxide or carbon dioxide [1]. The compounds within this group are of interest due to the various roles they play as pollutants in several different environmental contexts. On the ground level, they take part in photochemical ozone formation and are hazardous to human health due to toxicity and carcinogenity. At the level of the atmosphere and stratosphere, they contribute to the greenhouse effect and the destruction of the ozone layer. There are many possible sources of organic compounds to the atmosphere, both biogenic and anthropogenic, of which the evaporation of vehicle fuel is only one example. Given these considerations, it should be clear that the release of anthropogenic VOCs must be restricted as much as possible.

Evaporative emissions of VOCs from cars are partly caused by the evaporation of volatile fuel components [2]. Although VOCs can also escape into the environment as unburned fuel components through the exhaust pipe, or by release from the plastic, leather and rubber parts in the car, these two mechanisms of VOC release will not be further discussed here. Increasing temperature causes the fuel to be evaporated, and this can occur due to elevated ambient

temperature or by heat coming from the engine [3]. Without any means of release control, the vapours that build up in the fuel tank can escape into the atmosphere either by a slow bleeding manner, or in a fast manner during refilling of the tank where the fuel vapours are displaced by the rising liquid level.

1.1.2 Controlling evaporative emissions of VOCs

Due to the harmful effects of VOCs described previously, there is generally some form of standard in place in developed countries around the world regarding the amount of VOCs that can be released by evaporative emissions from motor vehicles [4]. However, as Liu et al. explains there are differences between U.S. and European standards, which are the two most common types. U.S. standards are generally more strict than their European counterparts and are only applied in North America, whereas the relatively less strict European standards are generally applied in many other developed countries around the world in addition to Europe.

The U.S.A. has a long history with evaporative emissions control going back to the 1960's and -70's, when this type of emissions control started to be implemented with the state of California at the frontier of this development [3]. At this time, motor vehicles began to be equipped with canisters that were filled with activated carbon (henceforth referred to as either the canister, carbon canister or activated carbon canister), in order to prevent release of fuel vapours. The working principle of these activated carbon canisters was, and is still to this day the following: Fuel vapours that build up are transported through the canister, and as they move through the packed bed of carbon inside they adsorb on the surface of the carbon particles. In this way the hydrocarbons in the fuel vapours are trapped. Subsequently, in what is called the purging of the canister, air is drawn through the carbon bed to desorb the trapped hydrocarbons, and the resulting fuel-air mixture is fed to the combustion engine where the hydrocarbons are burned. In this way the evaporative emissions from the fuel system in the vehicle are limited to a significant extent. A detailed description of the design and function of the carbon canister is presented under section 2.1.

1.1.3 The canister performance in relation to future developments

The purging of the canister requires that the combustion engine is running. As hybrid-electric vehicles are introduced to an increasing extent in the future, there will be fewer opportunities for purging due to increased downtime of the combustion engine in favor of electric operation. This, along with increasingly stringent requirements for limiting evaporative emissions will place increased demands on methods that efficiently purge the canister.

The physical processes of adsorption and desorption of hydrocarbons on the carbon inside the canister are exothermic and endothermic in nature respectively. This means that energy is released when a molecule adsorbs on the surface, and conversely energy input is required for a molecule to desorb from the surface. Additionally, the release and uptake of energy affects the temperature level in the bed, and thereby the capacity for adsorption of the carbon [5]. As a consequence, the thermal energy content inside and heat flows to and from the canister are of importance for the efficiency of the canister operation. Previous work has shown indications that the canister performance can be improved during purge by supplying heat to the system, as is presented in section 2.4. The advantage of using heat to achieve this can result from different factors. It is possible that a larger quantity of hydrocarbons can be removed from the canister for a given flow rate of purge air, or alternatively, a possibly smaller flow rate of air would be required when supplying heat to the canister in order to remove a given quantity of hydrocarbons during purge.

Given the potential advantages of supplying heat to the canister during purge operation, it is of interest to investigate these possibilities further. With the importance of heat transfer in mind, it is also desirable to obtain detailed information on temperature variations in multiple dimensions in a canister during its operation. However, developing and building multiple prototypes for testing is a time-consuming and costly procedure, and therefore it is suitable to apply computer aided engineering tools to model and simulate a corresponding system. Such a model can provide meaningful results regarding effects of varying different parameters, but only provided that it has been tested and validated against actual measured data to ensure it is sufficiently accurate. Furthermore, a model that can simulate the dynamic behaviour of the canister under different conditions can be useful for providing more detail to large-scale simulations of the system that surrounds it.

1.2 Problem statement

The aim of this thesis project is to build a transient simulation model of an activated carbon canister in purge operation, with the capability of modelling heat input to the purge air flow. Furthermore, the model should allow for 2D simulations to resolve time transients of radial heat transfer effects in relation to purge operation. This is intended to serve the purpose of building a more comprehensive understanding of the implications of using heat to improve the canister performance, and to aid in future developments of the the canister concept.

1.3 Objectives

To arrive at the intended outcome stated above, the specific objectives of this thesis project are formulated as follows:

- To develop a simulation model of a carbon canister with 2D-functionality in the commercially available software GT-SUITE
- To calibrate the model using data obtained via experiments on a corresponding experimental canister, and to compare the simulation results to experimental data
- To use the proposed model to investigate the influence of different heating configurations in a parameter study

1.4 Demarcations

This project does not include any studies of real canisters of the form in which they are mounted on actual vehicles. The model developed in this project is intended to aid the understanding of the effects of heat transfer and heat addition rather than to simulate the performance of an end-user product. Therefore, a simplified cylindrical geometry is adopted in this project for modelling and experimental testing. Furthermore, this study is focused on simulating the purge event, meaning that simulations of initial vapour loading onto the carbon are not performed to any significant extent. The two-dimensional modelling discussed in this study applies only to the carbon beds of the canister, thus no other part of the system is modelled in multiple dimensions. With respect to heat addition, this study does not consider direct heating of the carbon bed, and therefore only includes purge heating to the extent that the heat is supplied to the purge air flow. Finally, it is beyond the scope of this project to include the effects of of the real composition of the fuel vapours in the model, and consequently only a single representative fuel component is used to model the fuel vapours.

1.5 Methods

The study consists of mainly a modelling section and an experimental section. The modelling of the canister system is performed in the software GT-SUITE 2018 developed by Gamma Technologies. Supporting calculations are mainly performed in MATLAB R2015b developed by MathWorks.

The experiments in the study are performed by building an experimental test rig of a canister system with beds of activated carbon. Measurements of temperature at different positions in the carbon beds and the weight change of the canister are performed during adsorption and desorption, in order to obtain data with which the model can be calibrated and to which the simulated results can be compared.

Chapter 2

Background

This chapter provides a background to the problem considered in the present study. A description of the EVAP-system is given along with some considerations of emissions and fuel, and finally a survey of previous studies that have been performed on the canister.

2.1 The EVAP-system and the carbon canister

The carbon canister is part of what is referred to as the EVAP-system, which consists of the lines to the canister from the atmosphere and the fuel tank, and the line going from the canister to the engine air intake as shown schematically in Figure 2.1.

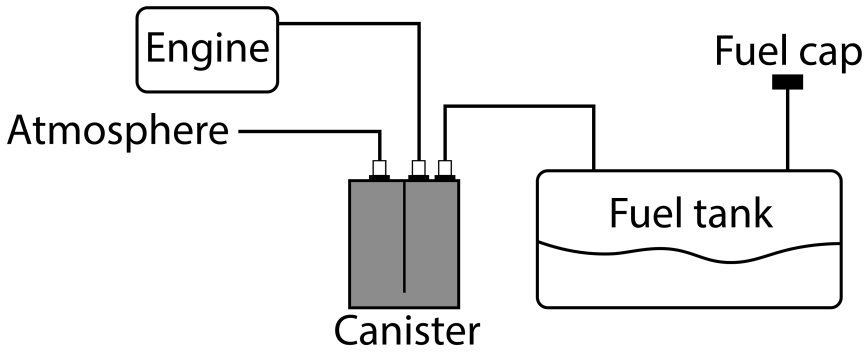

Figure 2.1: A simplified schematic description of the system surrounding the canister.

A schematic description of the principle function of the activated carbon canister is provided by Mohr [6]. Considering Figure 2.2, the canister has three openings to its surrounding system: the tank port which connects to the fuel tank where the vapours enter the canister (1), the at-

mospheric port where air can enter or leave the canister (3), and the purge port which connects the canister to the lines leading to the air intake on the engine (2).

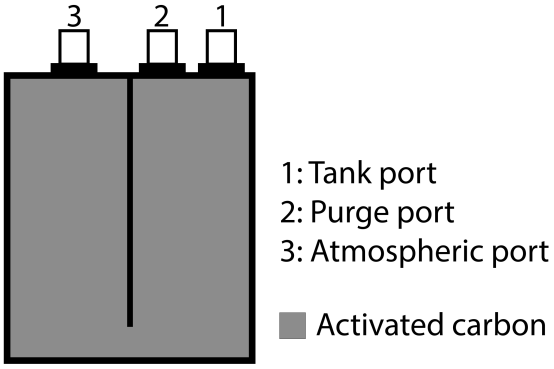

Figure 2.2: The activated carbon canister shown schematically.

When the temperature increases in the fuel tank there is a build up of pressure due to evaporation of the fuel, and as a consequence the air inside the tank is concentrated with hydrocarbons. To prevent damage to the fuel tank by the changes in pressure, the vapours must be vented from the tank in a way that does not allow release into the atmosphere [7]. The tank pressure causes the fuel-air mixture to migrate to the canister via the tank port, and as the hydrocarbons adsorb on the activated carbon the air is cleaned and passes through the atmospheric port [6]. The canister therefore serves as the preventive barrier for hydrocarbon release, and the process of fuel vapour adsorption on the activated carbon is referred to as loading. During purge operation the tank port is closed, and instead the purge port is opened where the relatively low pressure in the engine air intake causes a suction of fresh air into the canister via the atmospheric port. While the air is drawn through the activated carbon bed, the adsorbed hydrocarbons are desorbed and transported by the air flow to the engine where the mixture is used for combustion. Since the combustion engine runs on an air-to-fuel ratio that is managed by a control system, the fuel vapours that travel to the engine through the EVAP-system via the canister can be regarded as a disturbance to the engine system, which can potentially be significant [8].

There are different ways of designing the canister, with design choices including length-to-diameter (L/D) ratio and the number of cavities (compartments containing activated carbon that vapours must pass through). A study by Zhong et al. has shown that it is advantageous with respect to working capacity (the capacity for vapour capture during a loading-purge cycle) to design the canister with an L/D-ratio larger than 1, and to utilize a double-cavity design [9]. The authors claim that the advantage arises due to an increased travelling length of the vapours during adsorption. A similar result regarding the L/D-ratio was found by Johnson et al. in 1997 [10].

The advantages of using a large L/D-ratio may also include better plug flow characteristics and decreased effects of axial dispersion. Commercial canisters are often constructed with plastic housings, although the housing material constitutes a design choice with respect to material properties such as thermal conductivity, weight, permeability or diffusion properties and the cost of the material.

2.2 Emission types

As mentioned in section 1.1.1, there are different ways in which fuel vapours can escape, which is explained by Johnson et al. [3]. In what is referred to as diurnal emissions, the fuel tank of a parked vehicle is heated by the daily increase in temperature which causes production of vapours. Hot soak emissions occur just after a vehicle has been turned off, as there is still heat stored in the fuel system and engine which also causes vapour production. During the time that the vehicle is running, the fuel is warmed up by the heat generated during driving, which causes so-called running loss emissions. Resting losses can occur as well, which means that fuel vapours can diffuse through the material of the components used in the fuel system (these are however not captured by the EVAP-system). Refueling emissions occur on a relatively short time scale, where the liquid fuel that is pumped into the tank causes displacement of vapours [3]. The emissions from refueling are handled in different ways depending on the system used. Within U.S. regulation, in a so-called On-Board Refueling Vapour Recovery (ORVR) system the refueling vapours are captured by the vehicle (i.e. the canister), while in a Stage II system the refueling emissions are captured by the refueling station by suction from the fuel pump [11].

2.3 Petrol composition

The fuel considered in this study is petrol, which is used to power the internal combustion engine. Modern day petrol is a mixture of mainly aromatics, paraffins (alkanes) and olefins and contains a wide range (in the order of hundreds) of different hydrocarbons [12]. There are different categories of oil refinery products that go into the petrol mixture, for example straight-run petrol which is a direct product of distillation, and different forms of catalytically cracked petrol. The fuel is therefore a complicated mixture of many components.

For modelling cases such as the carbon canister it is not convenient to accurately represent the composition of petrol vapours, due to the complexity of the mixture. A suitable way to simplify the problem is to approximate the vapours from the fuel as being composed of pure n-butane, as was done by Sato and Kobayashi among others [7]. This approximation is reasonable since n-butane is in practice the dominant volatile component of petrol for vehicle use.

2.4 Survey of previous work

To establish a solid foundation for proceeding with a study on the activated carbon canister, it is necessary to review what work has been performed in the field previously. Studies of the factors that affect the canister system performance have been carried out by many authors, by using experimental and modelling approaches. A modelling attempt was presented by Lavoie et al. in 1996 where a one-dimensional model was constructed to describe adsorption-desorption dynamics inside a carbon canister [13]. Based on the results of the study, they concluded that the proposed model performed relatively poorly for the highest purge flow rates considered, and suggested that certain effects could be captured in a better way with a two-dimensional model. The model developed was used in an experimental study of canister performance by Johnson et al. in 1997, where hydrocarbon capture and emissions from canisters with different configurations were investigated [10]. They found among other things that using larger volumes of purge gas improved the canister performance.

In 2004, a two-dimensional transient model of adsorption and desorption of n-butane on activated carbon was developed by Bai et al. [14]. They report that the use of a Linear Driving Force model for the description of both mass and heat transfer is suitable for this kind of system, in combination with employment of the Dubinin-Polanyi theory of adsorption potential (these models are explained in chapter 3). They investigated how factors such as temperature and adsorbed amount varied in two dimensions, and found that the heat transfer at the wall caused a much lower temperature at the outer regions of the carbon bed, and more n-butane to be adsorbed in these regions. It can therefore be expected that radial effects of heat transfer are significant for accurate prediction of the canister behavior.

In an experimental study by Joyce et al. published in 1969, it was found that the working capacity for n-butane capture on activated carbon for a set of given test conditions could be improved by increasing the temperature of the carbon bed [15]. They highlighted the difference in temperature between the adsorption and desorption events and the volume of purge air as two parameters that are significant for the working capacity of activated carbon. The implications of heated purge air for the canister behavior was also discussed in a study published in 1967 by Clarke et al. [5]. While they found that the amount of hydrocarbons that were removed from the carbon bed increased for higher purge air temperatures, they highlighted the fact that the carbon bed temperature is elevated immediately after high-temperature purging, which would lead to a decreased adsorption capacity while the bed is warm. As a remedy, they proposed a sequence of purging with high- and low-temperature air. Further, in a study conducted by Bishop and Berg in 1987 a vapour canister heater was designed using PTC (Positive Temperature Coefficient) heaters, that was able to elevate the temperature of the incoming purge air [16]. In bench tests with canisters loaded with indolene as well as in tests on vehicles, it was shown that their vapour canister heater system could remove a significantly larger amount of hydrocarbons during purge

compared to experiments where heaters were not used. They also discussed the limitations of heating the carbon bed itself with the use of heating fins, and concluded that this method is not feasible due to the low thermal conductivity of the carbon bed (in the same order of magnitude as thermal insulating material).

Another possible method of increasing the canister performance was investigated and presented by Pittel and Weimer in 2004 [17]. In this study it was shown that high levels of vacuum during the purge event gave an increase in the working capacity of the canister. This was attributed largely to the decrease in what is referred to as the hydrocarbon heel (a residual amount of hydrocarbons that remains adsorbed on the activated carbon between purging and loading events) due to the vacuum.

In a previous master's thesis project carried out by Möller in 2016, a one-dimensional model of a simplified canister geometry was constructed in the software GT-SUITE by Gamma Technologies, and validated through experiments [18]. It was found in this study that radial temperature effects in the canister can be of importance and are not captured in a one-dimensional model, in agreement with the conclusions of Lavoie et al. from 1996 and Bai et al. from 2004. Möller's thesis serves to some extent as a starting point for this thesis project.

Based on the review presented, it is clear that there are precedents for modelling activated carbon canisters in one- and two-dimensional studies, and also for supplying heat to the canister to improve purge performance. However, the concepts of modelling two-dimensional heat transfer and purge heating do not seem to be frequently combined in previous works, which presents a motivation for carrying out such a study in this thesis project.

Chapter 3

Theory and modelling methods

This chapter presents the underlying theory needed to understand the modelling concepts and methods discussed in this study. The methods for modelling the physical behaviour of the canister are also presented.

3.1 Adsorption fundamentals and porous materials

The basic principles of adsorption are described by Seader et al. [19]. Molecules to be adsorbed (termed the adsorbate) are transferred selectively from the fluid phase (a gas in this context) to the surface of the solid phase (the adsorbent), where intermolecular forces act to keep the molecules bound to the surface. The bond between the molecule and the surface can be weak or strong depending on the type of adsorption that occurs. In what is referred to as physical adsorption (physisorption), the adsorbate is bound weakly to the adsorbent by intermolecular attraction forces of van der Waals-type, whereas in chemisorption the two are strongly chemically bonded to each other. In Figure 3.1, the potential energy of an adsorbate-adsorbent system as a function of the distance between the two is shown, as described by Thomas and Crittenden [20].

Adsorption results in a decrease in the potential energy, and thus thermal energy is released in the process. This heat release is referred to as the adsorption enthalpy or the heat of adsorption, and is shown on the potential curve in Figure 3.1. Thermodynamically, due to the decrease in free energy (ΔG_{ads}) and entropy (ΔS_{ads}) that occurs in the spontaneous adsorption of a molecule to a surface, it can be seen in the relation $\Delta G_{ads} = \Delta H_{ads} - T\Delta S_{ads}$ that the adsorption enthalpy ΔH_{ads} must be negative to satisfy a decreasing free energy, and so the adsorption process is exothermic (although some exceptions from this rule exist)[21]. The magnitude of the heat of adsorption that is released in a physical adsorption process is typically close to 20 kJ/mol (meaning that $\Delta H_{ads} \approx -20$ kJ/mol, with a negative sign to indicate an exothermic process). As a consequence of the heat release, the local temperature increases during the adsorption process.

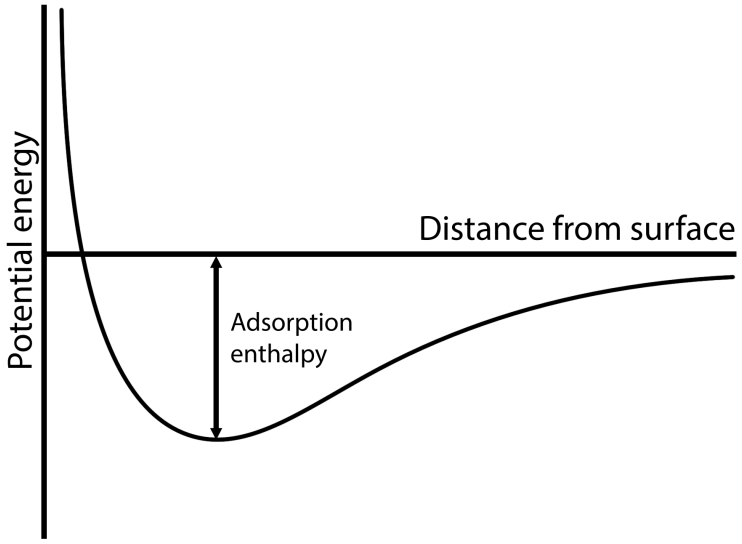

Figure 3.1: Schematic diagram of the potential energy of an adsorbate-adsorbent system as a function of the distance between adsorbate and adsorbent.

When the molecules desorb from the surface, a corresponding amount of heat is taken up by the surroundings and the local temperature is consequently decreased [22].

As discussed by Sircar and Cao, the adsorption enthalpy is usually quantified as an isosteric heat of adsorption, which gives the amount of heat released per unit amount of adsorbed molecules at a fixed coverage of adsorbate on the solid material [23]. One reason of obtaining it in this way is because the heat of adsorption can vary with the coverage on the adsorbent, if interactions between adsorbed molecules are significant. It can be obtained for specific adsorbate-adsorbent pairs by calculation from experimental adsorption data using thermodynamic relationships, or by direct experimental measurements using calorimetry. Fiani et al. studied the adsorption of n-butane on granular activated carbon, and found that the isosteric heat of adsorption was almost constant at approximately 22.1 kJ/mol for loadings between 0 and 0.3 grams of adsorbate per gram of carbon [24]. Furthermore, based on a study of the kinetics they concluded that the adsorption of n-butane on granular activated carbon exhibits behaviour that is consistent with physical adsorption. Chen and Yang reported an adsorption enthalpy for n-butane on activated carbon in the range 33-50 kJ/mol [25]. The different observed values of the adsorption enthalpy can be explained by the amorphous nature of activated carbon, as two carbons will not exhibit the exact same properties.

As mentioned previously, the bed inside the canister where the hydrocarbons adsorb is made up of porous activated carbon. A porous material can be described as a continuous solid phase

that contains a gaseous or liquid phase which makes up the pores in the solid, as explained by Liu and Chen [26]. According to their description, a porous material is porous by design, and so the pores are designed to serve some purpose in order to enhance the properties or performance of the material in a given context. In the case of adsorption, the porosity of the material serves to provide a large surface area per unit volume or mass of the solid, due to the large amount of pores of small diameters [19]. These pores are created in the so-called activation process, and there are different methods to achieve the porosity. Such methods include oxidation of the carbon material by mixing it with various chemicals, and high-temperature treatment of the carbon material with gases at temperatures in the order of $600 - 1200°\text{C}$ [27]. The resulting pores can have diameters roughly in the range of 1.2 - 20 nm, and the surface area of the activated carbon can range between 500 - 1500 m^2/g. Pores with opening sizes less than 2 nm are defined as micropores, and activated carbons can generally be considered to be microporous in their structure with surface areas depending on the activation process [28].

3.2 Rate of adsorption and the Linear Driving Force model

Modelling of an adsorption or desorption process relies on a sound description of the rates of those mechanisms. The intrinsic rate of adsorption can generally be said to be very fast in comparison to the rates of external and internal mass transfer, which can be regarded as the rate-limiting steps (while their relative importances can vary) [22].

As explained by Sircar and Hufton, the Linear Driving Force (LDF) model is a concept that describes the rate at which an adsorbate (pure or in mixture with an inert component) adsorbs to an adsorbent particle [29]. This model originates from the authors Gleuckauf and Coates in 1947, and is often used in situations related to adsorption column modelling due to its simplicity and its characteristics of being analytical as well as being physically consistent. In the study performed by Möller it was shown to give better results in relation to carbon canister modelling when combined with the Dubinin-Astakhov isotherm model (explained in section 3.3), compared to the commonly used Langmuir model for adsorption [18]. For this reason, the LDF model is used in the present study to represent the rates of adsorption and desorption inside the canister. It is formulated in the following way:

$$\frac{d\bar{c}(t)}{dt} = k_L \left[\bar{c}^*(t) - \bar{c}(t)\right] \tag{3.1}$$

where $\bar{c}(t)$ denotes the average concentration of the adsorbate at time t in the adsorbent particle, and $\bar{c}^*(t)$ is the average concentration of adsorbate in the particle at time t that would be observed if equilibrium conditions between the particle and the gas phase at the prevailing temperature and partial pressure of adsorbate were fulfilled [29]. k_L is an effective LDF mass transfer coefficient. Equation (3.1) implies that the adsorbate concentration in the solid increases by adsorption when the concentration is below that of equilibrium, and decreases by desorption

for concentrations larger than that of equilibrium. Instead of expressing the adsorbed amount in terms of concentration, one can write equation (3.1) using the dimensionless fractional coverage of adsorbate on the solid material:

$$\frac{d\bar{\theta}(t)}{dt} = k_L\left[\bar{\theta}^*(t) - \bar{\theta}(t)\right] \tag{3.2}$$

This model relies on the assumption that the temperature is uniform in one adsorbent particle, so there are assumed to be no gradients of temperature over the radius of that particle [29].

3.3 Describing adsorption equilibrium

The amount of adsorbate that is taken up by the adsorbent at equilibrium can be characterised in different ways. A common form of characterisation is by an adsorption isotherm, which relates the amount of adsorbed species to the partial pressure of that species in the gas phase at constant temperature [19]. Other forms of characterisation exist, such as isobars that relate the adsorbed amount to the temperature at constant pressure, and isosteres that describe how the partial pressure and temperature are related at constant amount of adsorbed species.

Different models exist for describing experimental isotherm data for adsorption. Such models are often restricted to certain intervals of pressure for validity, which must be accounted for when applying them to describe data [20]. A theory of adsorption equilibrium that is encountered within the framework of adsorption modelling on activated carbon is the Potential Theory developed by Polanyi, which is described as follows by Thomas and Crittenden. The concept is such that a surface of a solid is considered, and above this surface exist contours of equipotential energy ϵ. The volume of adsorbed species ϕ in the space between any potential surface ϵ and the surface of the adsorbent can be written as

$$\phi = qV_m$$

where q represents the adsorbed number of moles per unit adsorbent mass (mol/kg) and V_m is the volume per mole of adsorbed species (m^3/mol). It is possible to relate the volume of adsorbed species to the potential energy such that

$$\epsilon = f(\phi).$$

The energy ϵ is the work required to compress the gas phase from pressure p to the saturation pressure p_s, which means that for an ideal gas with volume v that is contained within an open system it can be written as follows:

$$\epsilon = \int_p^{p_s} v\, dp = RT \ln\left(\frac{p_s}{p}\right). \tag{3.3}$$

Hutson and Yang provides an overview of how this theory was adopted by Dubinin and his colleagues in the development of model equations for adsorption isotherms for microporous adsorbents [30]. As explained by Hutson and Yang, it is assumed in Polanyi's theory that a condensed adsorption film is created on the surface of the adsorbent inside its micropores via layer-by-layer coverage of the surface inside the pores. Dubinin in his adoption of this theory assumed that the mechanism of adsorption in micropores is instead due to the filling of the volume inside the pore, and not due to the layer-wise formation of a film on its surfaces. As a consequence there is a contradiction in the theoretical foundation, but Dubinin nevertheless used the theory to relate the quantity ϵ to the fraction of the micropore space occupied by adsorbate as

$$\frac{W}{W_0} = f\Big(\frac{\epsilon}{E}\Big)$$

where W is the adsorbed amount at the relative pressure of $\frac{p_s}{p}$, W_0 is the adsorbed amount at maximum capacity in the micropore system (also known as the limiting pore volume [25]) and E is a so-called characteristic energy of adsorption. This was further developed by Dubinin and Astakhov to include an additional parameter n, and by further manipulation one arrives at the Dubinin-Astakhov isotherm model equation for adsorption [30]:

$$\frac{W}{W_0} = \exp\Big[-\Big(\frac{\epsilon}{E}\Big)^n\Big] \tag{3.4}$$

This model equation has been found to work well for describing adsorption on microporous materials such as activated carbon [30]. However, a limitation of the Dubinin-Astakhov model is that it is in principle not valid for low loadings where $\frac{W}{W_0} \to 0$, because for low pressures it does not approach Henry's law [25]. The model was found by Möller to perform well for adsorption modelling on the same type of granular activated carbon considered in the present study, and consequently the model is used to describe adsorption equilibrium together with the LDF rate description in the study at hand [18].

Substituting ϵ in equation (3.4) with the expression on the right hand side in equation (3.3) and by letting the equilibrium fractional coverage be denoted as $\frac{W}{W_0} = \theta^*$, the following equation is obtained upon taking the average over a particle:

$$\bar{\theta}^* = \exp\left[-\left(\frac{RT\ln\left(\frac{p_s}{p}\right)}{E}\right)^n\right] \tag{3.5}$$

The temporal rate of change of the fractional coverage of the adsorbing species on the adsorbent can therefore be written as follows, by combining equations (3.2) and (3.5):

$$\frac{d\bar{\theta}(t)}{dt} = k_L\left[\exp\left[-\left(\frac{RT(t)\ln\left(\frac{p_s(t)}{p(t)}\right)}{E}\right)^n\right] - \bar{\theta}(t)\right] \tag{3.6}$$

The parameters k_L, W_0, E and n must be determined by calibrating against experimental data. The saturation pressure p_s can be found using the Antoine equation, which is a model based on three parameters that are fitted to experimental data on the variation of saturation pressure with temperature [31]:

$$\log_{10}(p_s) = A - \frac{B}{T + C} \tag{3.7}$$

where A, B and C are species specific parameters for a given interval of temperature, and T is temperature. The National Institute of Standards and Technology (NIST) provides values for the three parameters for n-butane at different ranges of temperature based on data provided by other authors, and these are presented for two relevant temperature ranges in Table 3.1 [32]:

Table 3.1: Antoine equation parameters for n-butane for two relevant temperature intervals as provided by NIST [32]. The parameters are based on units of pressure in bar and temperature in K.

Temperature range (K)	**A**	**B**	**C**	**Author**
195.11 - 272.81	3.85002	909.65	-36.146	Aston and Messerly (1940)
272.66 - 425.00	4.35576	1175.581	-2.071	Das and Reed et al. (1973)

3.4 Flow modelling methods

The adsorption-desorption processes inside the canister are coupled with the flow behaviour of the gas phase, and for this reason it is necessary to take this into account in a representation of the system. The physical behaviour of the canister system includes fluid flow in pipe parts as well as the phenomena that occur in flow through a packed bed of solid particles. The methods for modelling the physics of these flow situations are presented below.

3.4.1 Governing equations for one-dimensional fluid flow in pipes

GT-SUITE is in essence a one-dimensional simulation software, for which reason the governing equations for fluid flow are solved in one spatial dimension and time. There are however some features provided in the software that allow modelling in multiple dimensions, see equation (3.15) and section 4.2.1. When solving the flow of a fluid in the software GT-SUITE, the domain where the flow occurs is discretised into a number of volumes in a staggered grid approach [33]. The resulting grid consists of discrete volumes and the boundaries between those volumes. In each volume, the values of scalar quantities such as for example temperature and pressure are assumed uniform, and in the staggered grid these are calculated in the centre of the respective volumes. The values of vector quantities such as velocity and mass fluxes are calculated at the boundaries between the different volumes.

In general, the governing equations that represent the flow of a fluid are the equations for mass, momentum and energy. When applied to a discretised domain as described above, they can each be written according to the equations below [33]. Beginning with the conservation of mass:

$$V\frac{d\rho}{dt} = \sum_i \Big(\rho A_c u\Big)_i \tag{3.8}$$

where V is the volume of a discrete volume, ρ is the density of the fluid, i is the index denoting each boundary, A_c is the cross sectional surface area and u is the velocity at boundary i. The discretised equation for momentum is as follows:

$$\frac{d}{dt}\Big(\rho A_c u\Big) = A_c\frac{dp}{dx} + \frac{1}{dx}\sum_i \Big(\rho A_c uu\Big)_i - \frac{1}{dx}4f_f\frac{\rho u|u|}{2}\frac{A_c dx}{D_{eq}} - \frac{1}{dx}K_p\Big(\frac{1}{2}\rho u|u|\Big)A_c \tag{3.9}$$

where dp is the differential of pressure over the length dx of the discrete volume, f_f is the Fanning friction factor, D_{eq} is an equivalent diameter and K_p is a coefficient of pressure loss, e.g. due to bends and restrictions. The energy equation is written in terms of the specific enthalpy as follows:

$$\frac{d}{dt}\Big(\rho HV\Big) = \sum_i \Big(\rho A_c uH\Big)_i + V\frac{dp}{dt} - h_w A_w\Big(T_f - T_w\Big) \tag{3.10}$$

where H is the total specific enthalpy, h_w is a fluid-to-wall convective heat transfer coefficient, A_w is the surface area for heat transfer at the walls, T_f and T_w are the fluid and wall temperatures respectively. In an implicit method, the above equations are solved for all volumes simultaneously in an iterative manner at the next time step [33].

3.4.2 Governing equations for packed bed transport modelling

Special considerations are required for the description of momentum, heat and mass transport for flow through a packed bed of solid particles. A randomly packed bed has a large number of macroscopic tortuous openings which are difficult to account for in an exact manner. Empirical correlations in terms of dimensionless quantities describing momentum, heat and mass transport are commonly used to describe packed bed flow.

A packed bed causes frictional momentum loss as the fluid flows through it, which gives rise to a pressure drop. The pressure drop can be related to the Reynolds number in the bed, which in GT-SUITE is defined for a general geometry such as a packed bed as [34]

$$Re_b = \frac{D_p}{1-\varepsilon_b}\frac{\rho\varepsilon_b u_{is}}{\mu} \tag{3.11}$$

where Re_b denotes the packed bed Reynolds number, D_p is an effective particle diameter, ε_b is the bulk void fraction of the packed bed, u_{is} is the interstitial fluid velocity and μ is the fluid

dynamic viscosity. The effective particle diameter in equation (3.11) is calculated based on the void fraction and the specific surface area S (total particle surface area per volume of the bed) as

$$D_p = \frac{6(1-\varepsilon_b)}{S} \tag{3.12}$$

The frictional losses over the bed can be described using a well known and commonly adopted formulation due to Ergun in 1952, in which a friction factor f is calculated using the Reynolds number [35]. The Ergun equation in the following form is suggested by Gamma Technologies for packed bed geometries in GT-SUITE [34]:

$$f = \Big(\frac{1-\varepsilon_b}{2\varepsilon_b^2}\Big)\Big(\frac{150}{Re_b} + 1.75\Big) \tag{3.13}$$

The pressure drop over the bed is related to the friction factor as

$$f = \frac{-\Delta p}{L}\frac{D_p}{\rho u_s^2}\frac{\varepsilon_b^3}{1-\varepsilon_b}$$

where Δp is the pressure drop over the length L, and u_s is the superficial fluid velocity [35]. The Ergun equation is valid for laminar and turbulent flow conditions, making it a simple and useful description of the momentum effects on the flow through a packed bed.

Balance equations for the solid and gas phase energy need to be solved, and these equations are as follows, beginning with the solid phase energy equation [34]:

$$\Psi\frac{dT_s}{dt} = \frac{d}{dz}\Big(F_s\lambda_s\frac{dT_s}{dz}\Big) + hS\Big(T_f - T_s\Big) - \sum_k \Delta H_{R,k} r_k + \frac{Q}{V} + h_{ex}S_{ex}\Big(T_{ex} - T_s\Big) \tag{3.14}$$

where Ψ is the effective heat capacity per reactor volume, T_s is the solid phase temperature, F_s is the solid fraction of the bed, λ_s is the solid phase thermal conductivity, h is the interphase convective heat transfer coefficient between gas and solid, $\Delta H_{R,k}$ is the enthalpy of reaction k, r_k is the rate of reaction k, Q is a power source, h_{ex} is the convective heat transfer coefficient on the external boundary, S_{ex} is the external vessel surface area per vessel volume and T_{ex} is the external temperature.

In the two-dimensional case where heat transfer is solved in the radial direction of the packed bed as well, the following formulation is used to express the heat transfer between two adjacent volumes in the radial direction[1]:

$$q_{radial} = \lambda_s\frac{\Delta T_{s,radial}}{\Delta R_{radial}} \tag{3.15}$$

where q_{radial} is the heat flux between two radially adjacent volumes, $\Delta T_{s,radial}$ is the solid temperature difference between those volumes and ΔR_{radial} is the radial heat conduction length (i.e. the discretisation length in the radial direction). By discretising the radius into a number

[1] Jonathan Brown, Gamma Technologies, 2018-03-26. Personal communication.

of volumes m, a total number of $2m+1$ volumes are obtained across the diameter of the carbon bed, where the odd number accounts for the centre volume on the diameter. Given an axial discretisation that gives a number n of axial volumes, one carbon bed is therefore discretised into a total number of volumes $n \cdot (2m+1)$.

For the gas phase, the energy balance is written in the following way [34]:

$$\varepsilon_b \rho c_{p,f} \frac{d}{dt} T_f + \varepsilon_b \rho c_{p,f} u_{is} \frac{d}{dz} T_f = hS\Big(T_s - T_f\Big) \tag{3.16}$$

where $c_{p,f}$ is the specific heat capacity of the fluid. The interphase convective heat transfer coefficient h is obtained from the Nusselt number Nu:

$$Nu = \frac{1}{1-\varepsilon_b} \frac{hD_p}{\lambda_f} \tag{3.17}$$

where λ_f is the fluid thermal conductivity. The Nusselt number was obtained in this study by using the Chilton-Colburn analogy, in which the following factor j_H for heat transfer can be written as [36]:

$$j_H = \frac{Nu}{Re_b Pr^{\frac{1}{3}}} \tag{3.18}$$

where Pr is the Prandtl number. For packed beds, the following expression for the j_H factor has been suggested by Bird et al. [37]:

$$j_H = 2.19 Re_b^{-\frac{2}{3}} + 0.78 Re_b^{-0.381} \tag{3.19}$$

Combining equations (3.18) and (3.19) gives

$$Nu = \Big(2.19 Re_b^{\frac{1}{3}} + 0.78 Re_b^{0.619}\Big) Pr^{\frac{1}{3}} \tag{3.20}$$

Taking an average value of the Prandtl number (here assumed to be 0.7) allows the Nusselt number (and by extension the heat transfer coefficient through equation (3.17)) to be expressed only as a function of the Reynolds number by equation (3.20).

The continuity and momentum equations for the flow in the packed bed are written as follows, starting with the continuity equation[2] [34]:

$$\frac{d\rho}{dt} + \frac{d}{dz}\Big(\rho u_{is}\Big) = 0 \tag{3.21}$$

The momentum equation is written as:

$$\varepsilon_b \frac{dp}{dz} + \varepsilon_b \frac{d}{dt}\Big(\rho u_{is}\Big) + \varepsilon_b u_{is} \frac{d}{dz}\Big(\rho u_{is}\Big) = -Sf \frac{1}{2} \rho u_{is}^2 \tag{3.22}$$

[2]Note: the equations solved in GT-SUITE are given only in a quasi-steady formulation in the reference [34]. In this report, these equations are presented in the transient form as recovered by noting the simplification for the quasi-steady formulation stated in the reference: $\frac{D}{Dt} \rightarrow u_{is} \frac{d}{dz}$

In addition, equations are solved to determine species mass fractions and coverages on the solid material. The mass balance for the gas phase species j is [34]:

$$\varepsilon_b \rho \frac{d}{dt}\left(\Omega_{f,j}\right) + \varepsilon_b \rho u_{is} \frac{d}{dz}\left(\Omega_{f,j}\right) = \sum_k \sigma_{j,k} r_k \tag{3.23}$$

where $\Omega_{f,j}$ is the mass fraction of species j in the fluid, and $\sigma_{j,k}$ is the stoichiometric coefficient of species j in reaction k (in this context, the adsorption reaction). A condition is imposed for the coverage at each active site that the sum of all species coverages should be unity:

$$\sum_j \theta_j = 1 \tag{3.24}$$

The rate of change of the coverage is determined by the reaction rate and the stoichiometry:

$$\Lambda \frac{d\theta_j}{dt} = \sum_k \Lambda \sigma_{j,k} r_k \tag{3.25}$$

where Λ is the density of active sites in the solid. The rate of the adsorption or desorption reaction relates back to the right hand side of equation (3.6).

Chapter 4

Experimental and simulation methods

This chapter presents the methods used for the experiments and simulations performed in this study. In general, the methods applied here are based on and expand upon those presented previously by Möller [18].

4.1 Experimental methods

The canister model equations discussed in chapter 3 rely on the unknown parameters k_L in equation (3.6) and the enthalpy associated with adsorption or desorption (the unknown aspect of the latter parameter is discussed further in section 4.2.3, and also in appendix D). These parameters can be calibrated if experimental data is available for transient thermal effects and canister mass change during loading or purging. Alternatively, k_L could possibly be estimated using correlations for an interphase mass transfer coefficient in packed beds as is done for interphase heat transfer in this study. The treatment of k_L and interphase mass transfer is described in section 4.2.1.

The experimental data mentioned above are not only important for calibration, but also for validation to ensure that the model is able to produce sound results. This section describes the procedures that were applied to obtain such experimental data.

4.1.1 Experimental canister test rig description

For the purpose of gathering experimental data during loading and purging cycles, an experimental carbon canister was constructed with the design shown schematically in Figure 4.1. It consisted of two cylindrical columns, each with an inlet plastic pipe section followed by a 0.5 L

bed of BAX1500 activated carbon pellets, held in place by perforated metal plates and plastic foam filter material at each end of the bed. The two columns were identical in design but flipped vertically relative to each other, with a connecting pipe allowing flow from one column to the other. To be consistent with nomenclature and taking purge mode as the reference case, the carbon bed on the left hand side of Figure 4.1 will henceforth be referred to as the first carbon bed (or carbon bed 1, CB1 in short), and the bed on the right hand side will be referred to as the second carbon bed (carbon bed 2, CB2). Measurements of the experimental canister are provided in appendix A.

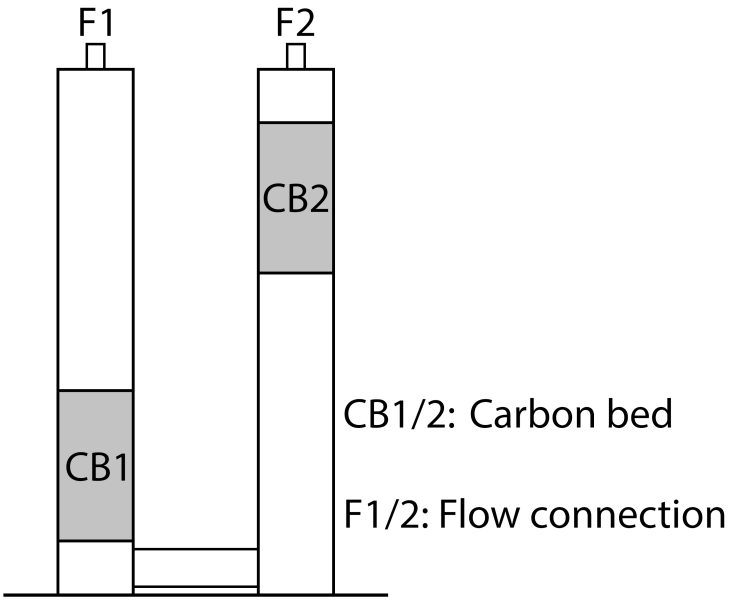

Figure 4.1: Schematic view of the experimental test rig of an activated carbon canister used for experiments.

There were multiple reasons for choosing this design. The main purpose of the design was to allow for heat input to the purge air flow before it came in contact with the activated carbon[3]. Furthermore, it was desirable to increase the level of flexibility regarding heat input to the canister, by allowing heat input to the purge air in two stages along the total carbon bed length rather than one stage only. In this way, the design was intended to allow for investigating the effects on the canister performance from varying the heat supply in the two stages relative to each other. Therefore, two separate carbon beds were used with pipe sections before each carbon bed inlet where heaters could be placed. The choice to arrange the pipes and carbon beds vertically was made to eliminate possible gravitational effects on the flow along the radii,

[3]It is however worth noting that purge heating experiments could not be performed later on in the study.

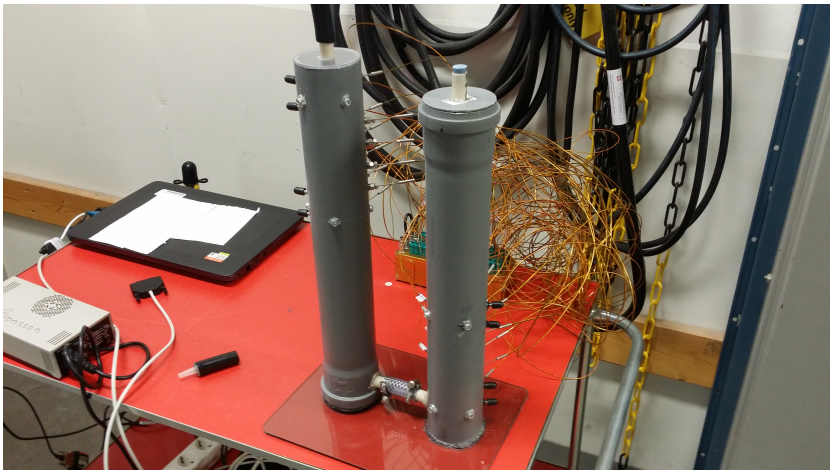

Figure 4.2: The experimental canister built according to the schematic. The carbon beds were fixed in the volumes enclosed by the metal screws on each pipe. Thermocouples were inserted into the carbon beds on the backside. The small metal pipes with black rubber caps on each carbon bed allowed for pressure drop measurements between those positions.

since this effect was shown by Möller to have some significance [18]. To reduce the height of the construction and increase stability, the pipes were arranged parallel to each other. According to the recommendations for the L/D-ratio presented in section 2.1, the carbon beds were designed with an L/D-ratio of 1.89.

The experimental canister was equipped with 12 thermocouples inside each carbon bed, to enable temperature measurements at different axial and radial positions during loading and purging. Additional thermocouples were added at the inlet and outlet of each carbon bed to allow measurement of the incoming and outgoing temperatures. The placement of thermocouples is presented in detail in Table A.1 in appendix A.

4.1.2 Pressure drop experiments

For the purpose of comparing the flow characteristics in the developed canister model to experimental data for validation, experiments were performed on the canister test rig to obtain pressure drops over five different lengths on the flow path. The positions for pressure measurements are shown in Figure 4.3.

The canister was connected from eight different positions to five pressure gauges, and the inlet on the canister was connected to a flow measurement rig. The positions over which to measure the pressure drops were chosen to give the following: i) the total pressure drop over the whole path from the first carbon bed inlet to the second carbon bed outlet, labeled ΔP_{1-8} ii)

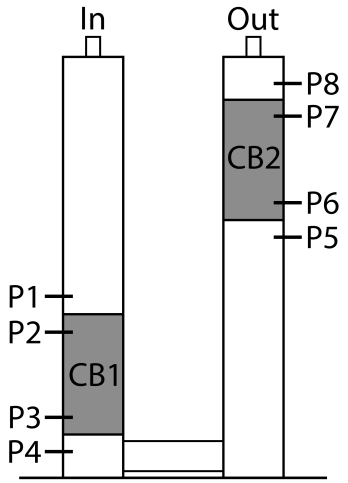

Figure 4.3: The positions for pressure measurements on the test rig, labeled P1-P8. The flow inlet and outlet for the pressure drop experiments are labeled In and Out.

the pressure drop over each carbon bed including the perforated metal plates and filter material at each end, labeled ΔP_{1-4} and ΔP_{5-8} respectively iii) the pressure drop over each bed not including the plates and filter material, labeled ΔP_{2-3} and ΔP_{6-7} respectively.

The flow measurement rig connected to the canister inlet was used to give flow rates of air through the canister, varying from 10 L/min up to 100 L/min at even increments of 10 L/min. The pressure drops were sampled after reaching steady values at each flow rate of air.

4.1.3 Loading experiments

To load the canister with fuel vapours before the purge event, experiments were performed where the canister was loaded with n-butane. The canister test rig was placed on a scale connected to a measurement computer by serial communication which sampled the canister weight over time. The canister was then connected to a mass flow controller which produced 40 g/h of n-butane in a 50/50 mixture by volume of n-butane and nitrogen gas. The flow from the mass flow controller was fed in at nipple F2 as seen in Figure 4.1 for the loading experiments, and the outlet at nipple F1 was connected to a dummy canister downstream which was placed on another scale. The system was configured so that the flow of n-butane and nitrogen stopped when the downstream dummy canister showed a loading of two grams, indicating that breakthrough had been achieved for the experimental canister. The temperature was measured continuously at all thermocouple positions throughout the loading experiments.

4.1.4 Purging experiments

When the experimental canister had been loaded until two grams of breakthrough was observed to the downstream dummy canister, the carbon beds were allowed to cool off to room temperature. The connection at nipple F1 was then removed and opened towards the atmosphere, and nipple F2 was connected to another flow channel on the mass flow controller. This configuration gave a suction of air through the canister from nipple F1 to nipple F2, giving a reversed flow relative to the loading experiments. The flow rate of air was set to approximately 23 L/min, and the flow was turned on for one hour during each purging experiment. Just as in the loading experiments, the temperature at all thermocouple positions and the canister weight were measured continuously during purging.

4.2 Simulation methods

Simulations of the canister purge event were performed in the software GT-SUITE developed by Gamma Technologies. In the software, a simulation model is built by using a set of pre-defined templates made by Gamma Technologies, from which objects can be created, configured and interconnected to suit the user's purpose. Examples of such templates are round pipes, flow splits, catalyst bricks and various boundary conditions. Settings for numerical solvers and time marching are available, with which a complete model can be assembled to simulate the transient evolution of the system that is studied. Different sensors and monitors can be used to observe and evaluate quantities of interest at different locations in the system. Simulating the canister means solving model equations (3.8)-(3.16) and (3.20)-(3.25) for the volumes of the discretised flow circuit created with the template objects.

4.2.1 GT-SUITE simulation model

In GT-SUITE, a 1D base model was created to represent a canister with two separate carbon beds, featuring possibilities for heating of the purge flow at each bed inlet. The underlying methods for representing the canister in GT-SUITE (e.g. choice of templates and various configurations) are largely based on and similar to the previous work performed by Möller [18]. Some differences between the previous and present simulation models are discussed in appendix D. The objects that were included are listed with descriptions in Table B.1 in appendix B. The layout of the simulation model in GT-SUITE is shown schematically in Figure 4.4.

The central objects of this model were the carbon beds in conjunction with surface reaction specifications and the heaters. These objects were meant to model the core functions of the experimental canister, which is described in section 4.1.1. The additional flow objects such as the pipes before, in between and after the carbon beds were included and configured to model the complete experimental canister to the furthest extent possible.

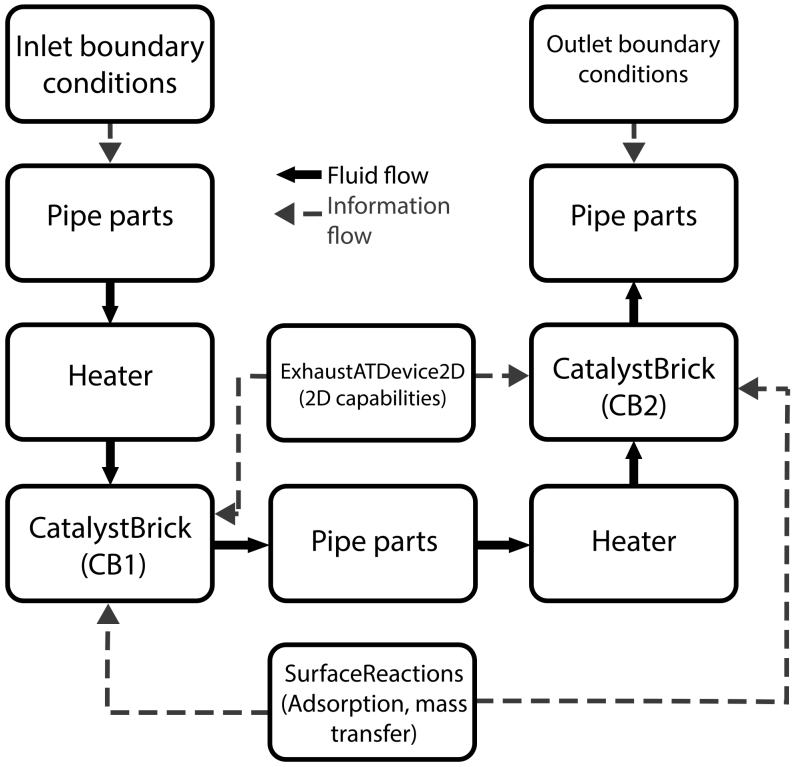

Figure 4.4: A schematic description of the layout and function of the GT-SUITE simulation model.

The carbon beds were modelled with the `CatalystBrick`-template, which models a catalytic converter geometry with characteristics according to user definition (e.g. square channels in a monolith or a packed bed). In this case, a "General Geometry"-setting was chosen which allows the input of settings that aim to model a packed bed of particles. These settings include specific area, solid fraction and functions for $f \cdot Re_b$ and Nu as functions of Re_b. The specific area and solid fractions were specified in accordance with material data for BAX1500 activated carbon provided by Ingevity[4]. The functions for $f \cdot Re_b$ and Nu were specified using equations (3.13) and (3.20). The density, thermal conductivity and specific heat capacity for the carbon beds were specified from the provided material data. The wall material properties were set to model the plastic pipes housing the carbon beds, with the specified properties presented in Table B.2 in appendix B.

Reaction specifications for desorption according to equation (3.6) and (3.7) were set up in the

[4]Timothy Byrne, Ingevity, 2018-03-08. Personal communication.

`SurfaceReactions`-template, which passes reaction and mass transfer information to the carbon bed objects. An `if`-statement with a temperature condition was incorporated to ensure that the appropriate coefficients from Table 3.1 were used for the Antoine equation at each instant. The details on how the expressions were entered into the template are described in appendix B.2. N_2 and n-butane were specified as the species concentrations to be solved for in space and time, although N_2 was considered inert and did not participate in any of the defined reactions. The capacity for loading of n-butane on the carbon was defined by an "Active site density"-setting in this template with units mol/m^3. This quantity was modelled by converting the value of W_0 obtained from the isotherm parameter fitting procedure (described in section 4.2.4) into units mol/m^3 with the molar mass of n-butane.

The `SurfaceReactions`-template provides an option for the treatment of interphase mass transfer through a "Diffusion"-setting. In the present model this was set to "Off", which means that the software assumes that there is no difference in species concentrations between the bulk gas phase and the surface of the solid material. Thus the effects of interphase mass transfer were instead completely attributed to the LDF mass transfer coefficient k_L in equation (3.6). The effect of changing the "Diffusion"-setting is discussed in appendix D. Intraparticle mass transfer limitations via pore diffusion were neglected in this model for simplicity, and this is discussed in section 6.5 along with the assumption of uniform intraparticle temperatures.

To raise the temperature of the purge flow, the heaters were modelled each as a single flow volume located before the respective carbon beds, configured to have heat sources with values specified through a parameter setting. Since they were represented by single volumes and the temperature is uniform throughout each volume, the transfer of the supplied heat to the flow was assumed ideal. Each heater volume was set up to be adiabatic to eliminate heat losses from those parts, therefore allowing accurate control of the heat input to the passing gas flow.

Initial conditions for temperature, pressure and gas composition were set for the purge event as 23 °C, 101325 Pa and a 50/50 vol-% mixture of N_2 and n-butane respectively. The inlet boundary conditions were set up with a flow rate of 23 L/min, a temperature of 23 °C and a pure N_2 composition. On the outlet the temperature, pressure and composition were set to 23 °C, 101325 Pa and pure N_2 respectively.

In order to extend the model to 2D and simulate heat transfer in the radial direction of the carbon beds, the `ExhaustATDevice2D`-template was used to give 2D-capabilities to `CatalystBrick`. This means that radial heat transfer is solved in the form of equation (3.15), and the temperature is potentially non-uniform over the radius as opposed to the 1D-case. The `ExhaustATDevice2D`-template was configured by setting the number of volumes that the radii of the carbon beds were discretised into. Deciding whether to use this functionality or not gives the user the ability to

choose between 1D and 2D resolution in the carbon beds.

4.2.2 Numerical setup

The governing equations for flow, friction and heat transfer presented in sections 3.4.1 and 3.4.2 were solved with an implicit solver setting, which applies sub-iteration to solve the quantities in the equations for the next time step. The size of the time step was specified as 0.02 seconds, but was adapted within the sub-iterations to ensure convergence. The equation associated with the reaction of desorption was solved implicitly using a backward differentiation formula setting. The discretisation length in the axial direction was specified as 5 mm, and in the radial direction the number of volumes was set to 9, giving a radial discretisation length of 3.88 mm for an inner diameter of 70 mm. The axial and radial discretisation lengths to use in the model were chosen so that the cumulative mass change of the canister during purge (the main result of interest) was sufficiently independent of the discretisation lengths, with respect to variation in the results and simulation time.

4.2.3 Calibration of unknown parameters

The `SurfaceReactions`-template in GT-SUITE requires a specification of the heat release or uptake associated with the change in coverage of n-butane on the carbon beds, through an "Enthalpy of formation"-setting for occupied active sites in units J/mol. The numerical value of this setting to be entered in GT-SUITE is not to be confused with the values of the enthalpy of adsorption suggested in the literature as mentioned in section 3.1, although they have the same basic physical significance. The enthalpy of formation was therefore treated as a calibration parameter in this study, which has been done previously by Gamma Technologies[5], as well as by Smith et al. [38]. The enthalpy of formation and the other unknown parameter, the LDF mass transfer coefficient k_L in equation (3.6), were calibrated to give the best possible fit of the model outputs to experimental data, obtained from the purging experiments carried out as explained in section 4.1.4. To calibrate k_L, the measured canister mass change due to n-butane desorption was used as a measurement of the reaction rate. The measured temperatures in the carbon beds were used as indications of heat uptake or release to calibrate the enthalpy of formation parameter.

The calibration was performed using the optimiser functionality available in GT-SUITE, which allows the user to search for an optimum of any specified output from the simulation model by setting up a factorial design with a desired resolution. The output to be optimised was specified as the sum of square errors between simulated and experimental data integrated over time for the following quantities: the transient mass change profile of the canister, the

[5]Jonathan Brown, Gamma Technologies, 2018-03-26, Personal communication.

temperature in the first carbon bed near the inlet, and the temperature in the second carbon bed near the outlet. Weighting coefficients were arbitrarily specified as 9 for the square error of mass change and 1 for each error of temperature to reflect the importance of the mass change as the primary model output. Initial test simulations of the purge event were performed to identify a suitable assumption of the initial coverage of n-butane on the carbon, and to form a starting point for the calibration parameters.

4.2.4 Fitting of isotherm parameters

Experimentally measured isotherm data for activated carbon of brand BAX1500 was provided by Ingevity[6]. The data contained equilibrium mass loading of n-butane on the carbon per unit bed volume at different sets of n-butane concentration and pressure. Such data was provided for the constant temperatures of 25 °C (in a pressure range of 0.0008-450 Torr) and 100 °C (with pressure range 1-10349 Torr).

The partial pressure of n-butane was calculated for each data point, and the saturation pressures at 25 °C and 100 °C were calculated with equation (3.7) using the parameters in the second row of Table 3.1. The Dubinin-Astakhov isotherm model equation in the following form was defined as a function in MATLAB:

$$W = W_0 \exp\left[-\left(\frac{RT \ln\left(\frac{p_s(T)}{p}\right)}{E} \right)^n \right]$$

where W and W_0 have units of g/L carbon. The MATLAB function `fminsearch` was used to find the minimum of the sum of the square errors between the modelled and experimentally measured values of W, by finding the optimal values of W_0, E and n at the temperature T:

$$solution\big(W_0, E, n, T\big) = \min\left(\sum_{j=1}^{m} \Big(W_{j,model}(T) - W_{j,experiment}(T) \Big)^2 \right)$$

where j denotes one measurement point, m is the number of measurement points and T is either 25 or 100 °C.

4.2.5 Pressure drop simulations

To compare the pressure drops produced by the model with the measured pressure drops over the experimental canister, simulations were performed with the canister model in 1D resolution not including any adsorption, desorption or heating of the canister. The inlet flow rate of nitrogen was stepwise increased from 10 to 100 L/min allowing for a stable pressure drop to be obtained at each step. To obtain comparable data for the pressure drops caused only by the carbon, the lengths of the carbon beds in the GT-SUITE model were adjusted to match the lengths of the

[6] Timothy Byrne, Ingevity, 2018-02-28. Personal communication.

inner measurements P2-P3 and P6-P7 shown in Figure 4.3. For the pressure drop P1-P8 the beds were adjusted back to their original lengths to match the dimensions of experimental canister.

4.2.6 Parameter study - simulated cases

After calibration of the model had been performed, the model was used to simulate cases of different purge heating configurations, canister geometries and heat transfer properties in a parameter study. All cases are presented together in Table 4.1, with the calibrated base case model labeled as case 1.

Using 2D resolution, purge heating simulations were performed using the cumulative purged mass of n-butane after one hour as the primary output to be compared between different configurations. In cases 1-11, the effect of the total amount of heat supplied was investigated by varying the degree of heat input to the canister, with equal sources (Q_{CB1} and Q_{CB2}) at both heater locations. To investigate the influence of unequal heating of the carbon beds on the purged mass, cases 12-20 were simulated where the total heat supply (Q_{tot}, equal to $Q_{CB1} + Q_{CB2}$) to the canister was fixed at 80 W (corresponding to case 5), and the relative heat inputs to the carbon beds (Q_{CB1} and Q_{CB2}) were varied.

The influence of modelling in 2D compared to 1D was also evaluated by varying the diameter (D_{bed}) of the carbon beds in a case of unheated purge, with case labels 21-26 which were simulated in both 2D and 1D. To investigate how the radial heat transfer is affected by changes in the convective heat transfer on the external boundary and the heat conduction in the carbon bed, the external convective heat transfer coefficient (h_{ex}) and the carbon bed thermal conductivity (λ_s) were varied as shown in cases 27-28.

Table 4.1: Simulations of the purge event performed in the parameter study, with cases of different configurations of heating before each carbon bed, different diameters and heat transfer properties. Subscript 1 denotes the corresponding value in case 1.

Case	Q_{CB1} **(W)**	Q_{CB2} **(W)**	Q_{tot} **(W)**	D_{bed} **(mm)**	$h_{ex}/h_{ex,1}$	$\lambda_s/\lambda_{s,1}$
1	0	0	0	70	1	1
2	10	10	20	70	1	1
3	20	20	40	70	1	1
4	30	30	60	70	1	1
5	40	40	80	70	1	1
6	50	50	100	70	1	1
7	60	60	120	70	1	1
8	70	70	140	70	1	1
9	80	80	160	70	1	1
10	90	90	180	70	1	1
11	100	100	200	70	1	1
12	80	0	80	70	1	1
13	70	10	80	70	1	1
14	60	20	80	70	1	1
15	50	30	80	70	1	1
16	40	40	80	70	1	1
17	30	50	80	70	1	1
18	20	60	80	70	1	1
19	10	70	80	70	1	1
20	0	80	80	70	1	1
21	0	0	0	35	1	1
22	0	0	0	70	1	1
23	0	0	0	105	1	1
24	0	0	0	140	1	1
25	0	0	0	175	1	1
26	0	0	0	210	1	1
27	0	0	0	70	100	1
28	0	0	0	70	1	100

Chapter 5

Results

This chapter provides the results obtained from the experimental study, as well as results from the simulations with the formulated model in GT-SUITE. Whenever normalised positions are used in the presentation of temperatures at certain points, in the axial direction 0 corresponds to the inlet and 1 to the outlet of each carbon bed in the purging case (meaning the flow direction is from the first to the second carbon bed). In the radial direction, 0 corresponds to the centre of the diameter and 1 to the outer boundary at the plastic housing.

5.1 Experimental results

In this section the results from the pressure drop measurements on the experimental canister test rig are presented, as well as results from the loading and purging experiments.

The pressure drops measured over distances P1-P8, P2-P3, P1-P4, P5-P8 and P6-P7 as explained in section 4.1.2 at flow rates of 0-100 L/min are presented in Figure 5.1. All measured pressure drops increase non-linearly with increasing flow rate of air. The magnitudes of the pressure drops over P1-P4, P2-P3, P6-P7 and P5-P8 are all similar while the total pressure drop over P1-P8 is larger.

In Figures 5.2a-b and d-e, the transient temperature profiles for loading and purging experiments respectively are shown at different axial positions of the carbon beds, at the centres of the bed diameters. The observed sequences of rises and drops of temperature show the plug flow characteristics of the canister and the reversed flow between the loading and purging cases. Figures 5.2c and f show the profiles of cumulative mass change of the canister during loading and purging. In the loading case, the canister gains mass at a constant rate of approximately 40 g/h until the supply of n-butane is cut off. During purge, the decrease in mass is quickest in the beginning and takes on an approximately linear profile after 20 minutes.

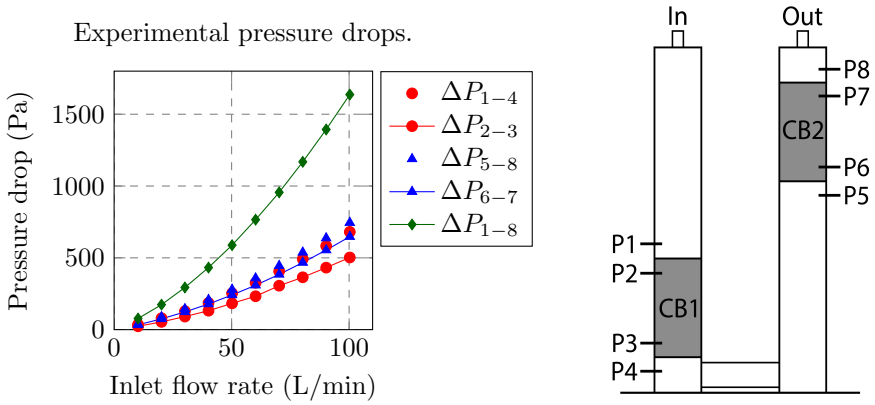

Figure 5.1: Experimentally measured pressure drops at varying flow rates in the canister test rig, over the distances shown in the schematic to the right.

As a representative result of the temperature effects in the radial direction during loading and purge, Figures 5.3a-b show the measured transient temperature profiles at three radial positions located at one axial position in the second carbon bed. At the peak temperature, a difference of approximately 20 °C is observed over the radius in the loading case. During purge, the largest temperature difference observed is approximately 12 °C.

5.2 Results of modelling and simulation

This section provides the results obtained from the modelling study. This includes the Dubinin-Astakhov model parameter fitting, the modelling of the packed bed pressure drop, the results of the calibration of the 2D canister model and the simulated cases of the parameter study.

5.2.1 Isotherm model parameters

Based on the experimental isotherm data gathered by Ingevity, the parameter fitting as described in section 4.2.4 was performed using the data sets with constant temperatures of 25 °C and 100 °C, thereby giving two sets of parameters. The parameter set that was found to give the best fit to the 25 °C-isotherm data is given in Table 5.1, along with the mean signed deviation (MSD) obtained when the parameter set was used to model the equilibrium loading at 25 °C and 100 °C. With $W_0 = 191.5$ g/L carbon, the active site density in the carbon was calculated to be 3295 mol/m^3. The presented parameters and active site density were then used in the canister model.

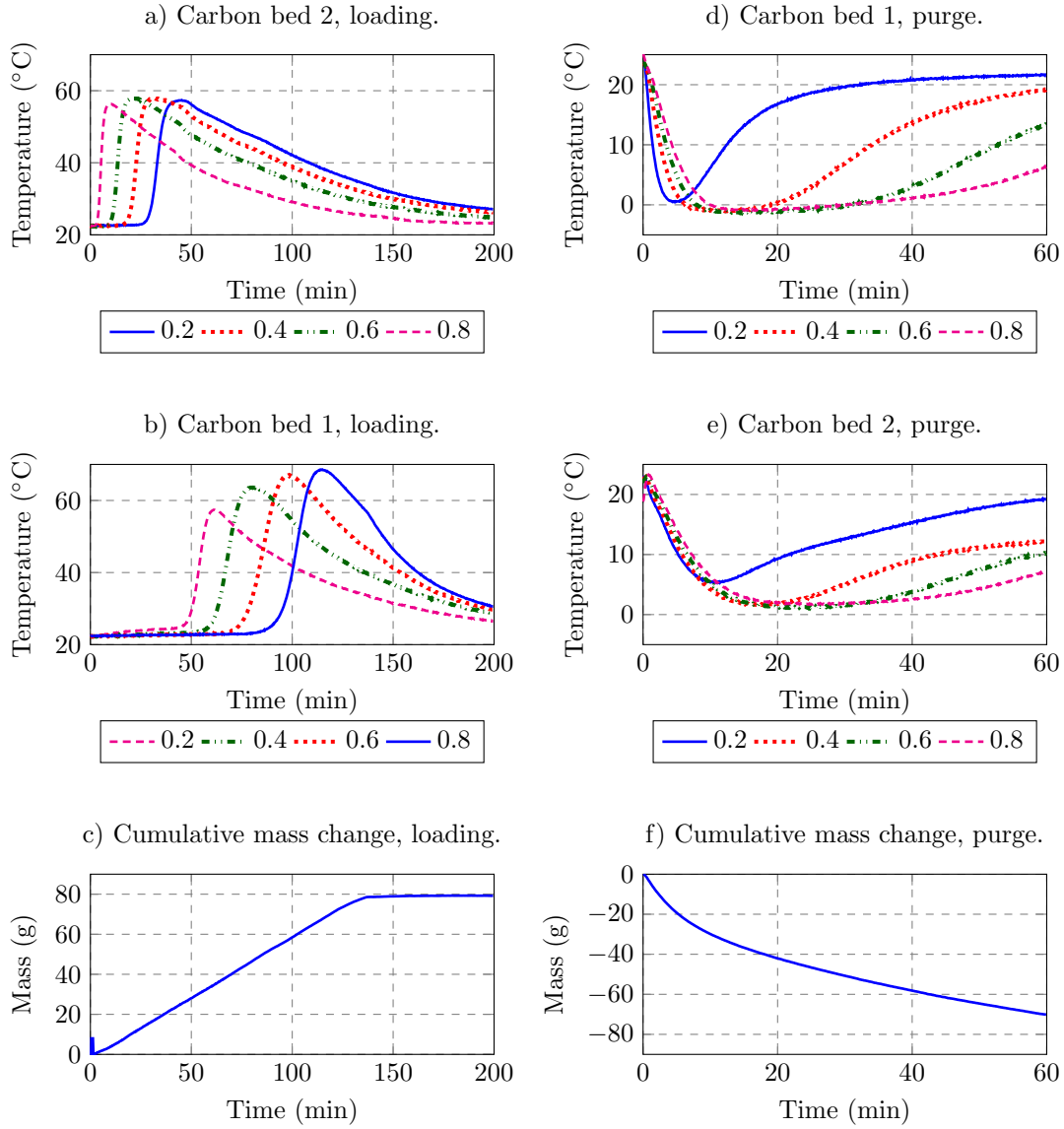

Figure 5.2: Experimentally measured profiles of temperature in the axial direction (centre radial position) of the carbon beds and cumulative mass change during loading and purging. The legend numbers correspond to the normalised axial positions of the thermocouples, 0 and 1 corresponding to inlet and outlet respectively.

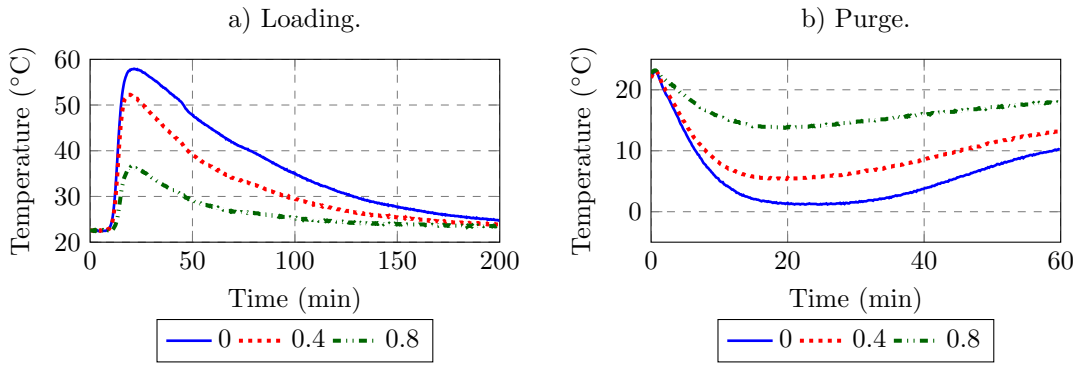

Figure 5.3: Experimentally measured temperature profiles during loading and purge, in three normalised radial positions along the same axial position in the second carbon bed. Position 0 corresponds to the carbon bed centre and 1 corresponds to the radial position farthest from the centre.

Table 5.1: Fitted parameter values for the Dubinin-Astakhov isotherm model based on experimental isotherm data given at 25 °C, along with the mean signed deviation of the modelled data from the experimental data.

W_0 **(g/L)**	E **(J/mol)**	n **(-)**	**MSD 25 °C (g/L)**	**MSD 100 °C (g/L)**
191.50	18422	1.43	-0.0853	1.1986

5.2.2 Pressure drop modelling

The results of the pressure drop modelling compared to the corresponding experimental results are presented in Figure 5.4. As seen, the packed bed pressure drop modelling approach produces results similar to the measured data at low flow rates of air, while at higher flow rates approaching 100 L/min the model begins to underestimate the pressure drop. The error between the simulated and measured drop in pressure caused only by the carbon shown in Figure 5.4a-b is smaller for the first carbon bed compared to the second.

5.2.3 The calibrated canister model

For an assumed uniform initial coverage of 0.82 in the purging case, k_L and the enthalpy of formation for occupied active sites were calibrated against the experimental data shown in Figure 5.2d-f. The resulting parameter values that were found to give best possible fit of the simulated results to the experimental data were $k_L = 0.0025$ s^{-1}, and an enthalpy of formation of -155 kJ/mol. In Figures 5.5 and 5.6 the calibrated model output is compared to said experimental data, with temperatures in the axial and radial directions as well as the purged mass of n-butane.

The simulated transient profiles of temperature in Figures 5.5a-d generally have similar mag-

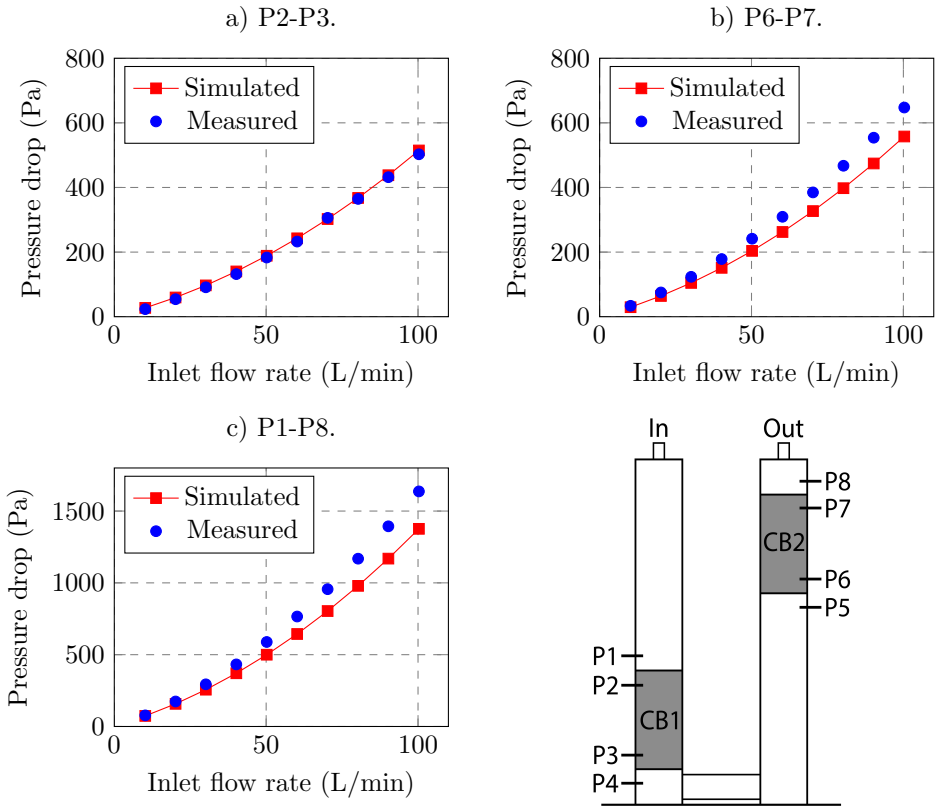

Figure 5.4: Simulated and measured pressure drops over the carbon beds compared to the corresponding experimentally measured data.

nitudes of the resulting minimum temperature to the experimental data, with the exception of the inlet to CB1. A varying agreement is observed in the time at which the minimum temperature is obtained. After the occurrence of the minimum temperature, the simulated temperature rises more quickly than the measured temperature. For the profile of mass change however, Figure 5.5e shows agreement between the simulated and experimental results corresponding to errors of 4 grams at most.

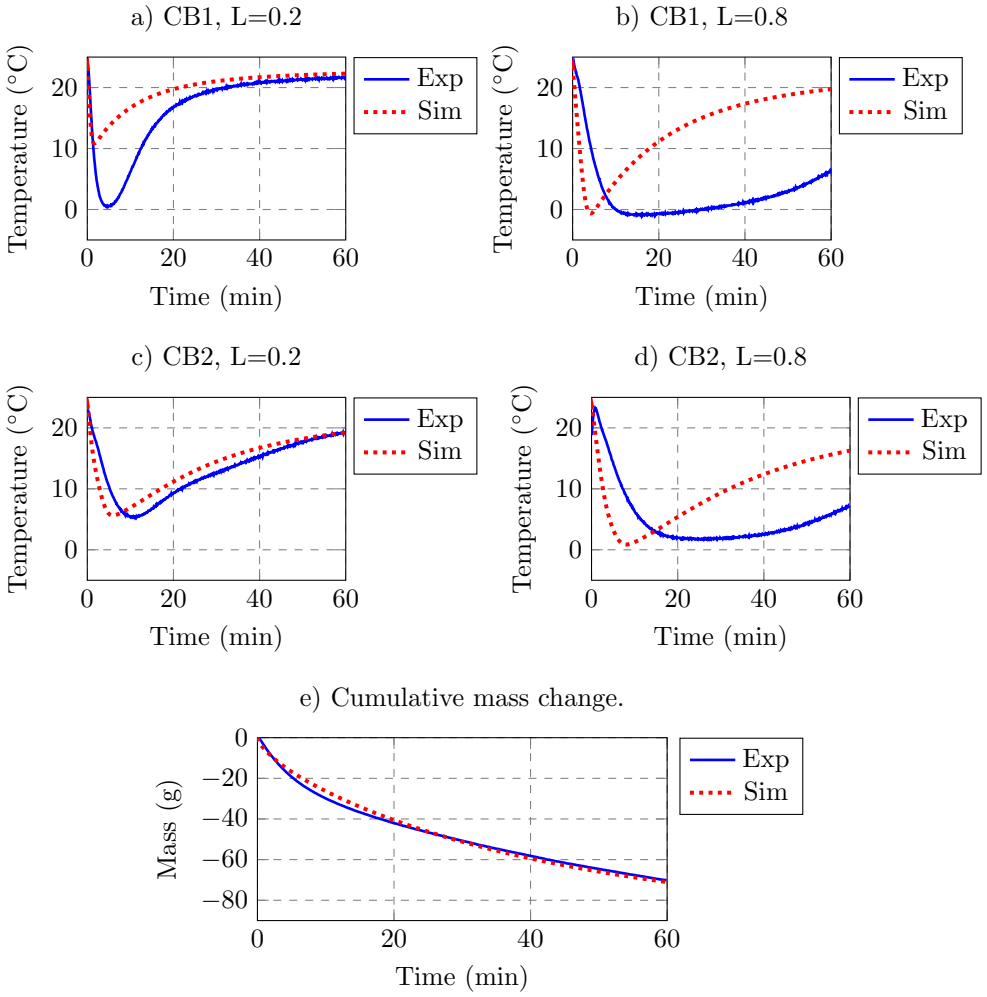

Figure 5.5: Simulated temperature profiles in the carbon beds at two normalised axial positions (L=0.2 and 0.8) in each bed along the radial centre, along with the simulated profile of mass change. The simulated results are compared to the corresponding experimental data.

Regarding the radial temperature effects, the calibrated model predicts the temperature at different points on the radius with varying accuracy relative to the measured temperatures as

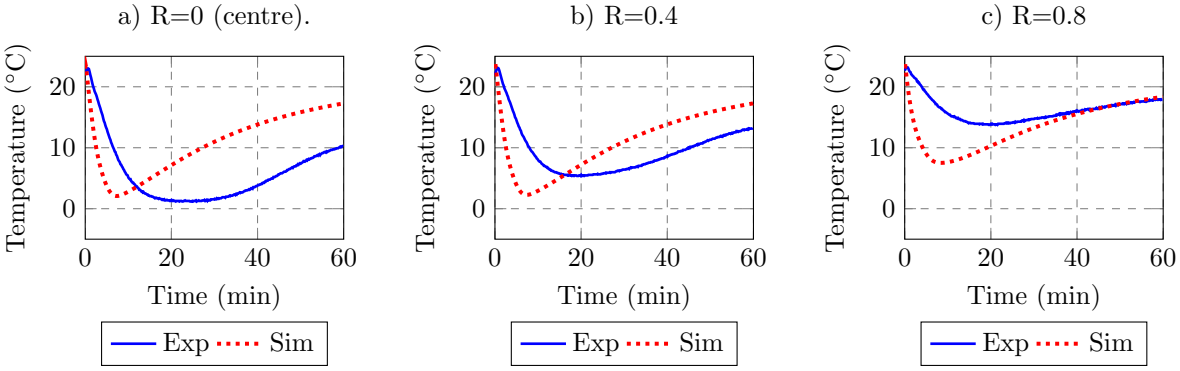

Figure 5.6: The simulated profiles of temperature at three radial positions at one axial position in the second carbon bed, compared to the corresponding experimental data. The position R signifies the normalised radial position with 0 corresponding to the centre of the bed.

seen in Figure 5.6. Closest to the wall (corresponding to R=0.8) the model predicts a minimum temperature of about 8 °C compared to the measured minimum of about 14 °C. The simulated change in temperature is more rapid compared to the experimental temperature change, which applies generally on the points in the radial as well as the axial direction.

5.2.4 Results from the parameter study

Several purging events were simulated with varying heat inputs to the purge flow, according to cases 1-11 in Table 4.1. The results expressed in terms of the canister mass change are presented in Figures 5.7a-b. As seen in Figure 5.7a, there is an increase in the mass of n-butane that can be purged during a given time when the total heat input is increased. The extra amount of purged n-butane achieved at each increment is decreased as the total heat input increases. Figure 5.7b shows that the initial rate of purge of n-butane is significantly increased when heat is supplied. For a given amount of purged n-butane, the time required to achieve said amount is significantly reduced when heat is supplied. Shown in Figure 5.7c is the coverage of n-butane on the carbon at the first discrete volume in the first carbon bed which is closest to the inlet of the purge flow. As seen, the coverage does not decrease below 20 % in the unheated case for the simulated duration of purge, whereas for the largest heat input the coverage approaches near-zero values.

For cases 12-20 the relative heat inputs before the two carbon beds were varied at a fixed total heat input. Figure 5.8 shows that the model predicts a decrease in the amount of n-butane that can be purged during a given time when the total heat input is shifted towards the heater located at the second carbon bed, farthest from the canister inlet in purge mode. Comparing the data point corresponding to heat input only to the first carbon bed (0 % to CB2 in Figure 5.8) to the data point in Figure 5.7a with 80 W of total heat input, a slight increase is observed when heat is supplied only before the first carbon bed.

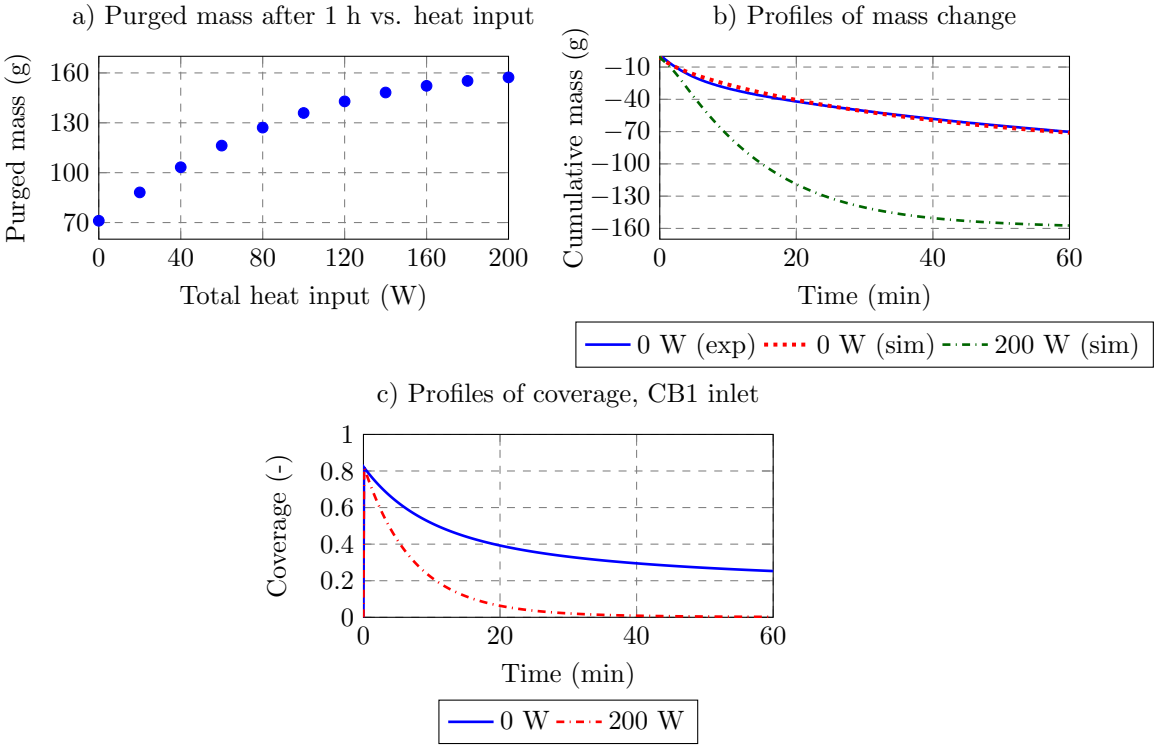

Figure 5.7: The total purged mass after one hour for the simulated cases 1-11 with varying total heat input to the canister. For the lowest and highest heat inputs, the simulated profiles of cumulative purged mass of the canister compared to the measured mass change with zero heat input are shown, as well as the simulated profiles of inlet coverage.

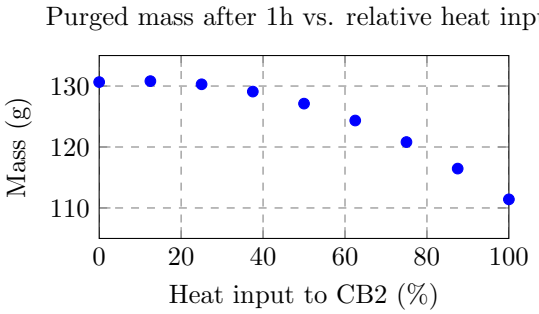

Figure 5.8: Simulated mass change after one hour of purge for cases 12-20 with varying relative heat input between CB1 and CB2, at a constant total heat input of 80 W.

Cases 21-26 were simulated in both 2D and 1D to reveal the effect on the results of simulating

in 2D compared to 1D. As seen in Figure 5.9, the two approaches produce similar results for small diameters of the carbon beds. When the diameters are increased, the 2D and 1D simulation results begin to diverge from each other, with the 1D model predicting a larger purged mass after a given time of purge compared to the 2D model.

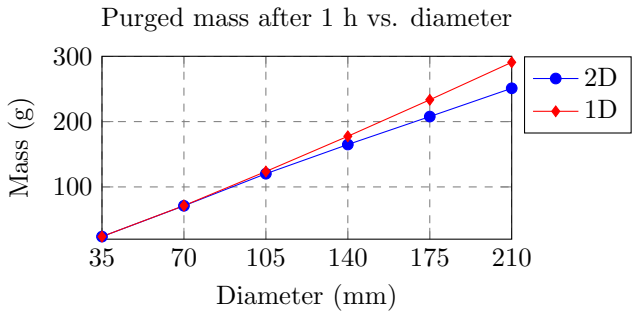

Figure 5.9: The simulated purged mass of n-butane after one hour at different diameters for cases 21-26, with a comparison between 1D and 2D simulations.

In an effort to reveal which type of heat transfer limits the radial temperature effects, cases 27-28 were simulated in which the convective heat transfer coefficient on the external boundary and the carbon bed bed thermal conductivity were increased by a factor 100 respectively. Figure 5.10 shows that the change in temperature in one of the middlemost radial positions is largest when the thermal conductivity of the carbon beds is increased. A relatively small change in temperature is observed when the external heat transfer is increased.

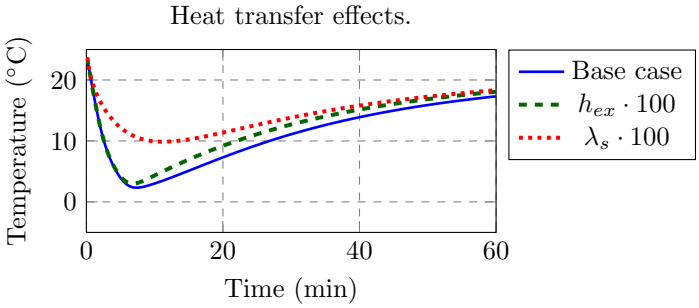

Figure 5.10: Simulated temperature profiles at a fixed normalised axial and radial location of L=0.6 and R=0.4 in the second carbon bed, for cases of increased external boundary heat transfer and carbon bed thermal conductivity as in cases 27-28.

Chapter 6

Discussion

In this chapter, the methods and findings from the experimental and modelling studies are discussed, as well as possibilities and suggestions for further studies.

6.1 Evaluation of experimental methods

A major reason behind the overall design of the experimental canister was the intended ability to mount heaters in the pipe sections leading to the carbon bed inlets, and subsequently perform experiments with heated purge air. Limitations during the project resulted in a need to put these planned experiments aside. Considering that experiments could only be performed without heated purge air, the design with two carbon beds is meaningless in the experimental study. A less complicated design for the purpose of modelling a canister without interstage heating would contain only one carbon bed, as was done by Möller [18]. A possible alternative could have been to build several experimental canisters equal in design but of varying diameters, to further investigate the radial temperature effects during the canister operation.

The loading and purging experiments were performed under fixed conditions for each run. All loading experiments were performed by loading the canister at 40 g/h of n-butane until a breakthrough of 2 grams to a downstream canister was observed. This is a standardised way of loading real canisters when evaluating their performance in the industry. However, for modelling purposes like in the present study, this method is problematic since the canister is not loaded to saturation with butane once the breakthrough occurs (this can be seen in Figure 5.2c, where the constant mass gain rate changes abruptly due to the n-butane flow being cut off). As a consequence, the n-butane coverage on the activated carbon is likely nonuniform throughout the carbon bed length at the time of breakthrough. In the present experimental method, the profile of coverage on the carbon after a loading event is unknown.

A more appropriate experimental method would be to always load the experimental canister until a sufficiently uniform axial profile of coverage is obtained. In order to judge when such a profile has been obtained, additional analysis techniques could be used such as gas chromatography or mass spectrometry. Such techniques could for example allow evaluation of the n-butane concentration at the canister outlet over time. One could also simply compare the rate of mass change of the downstream dummy canister to the feed rate of n-butane. The degree of coverage after loading and before purging could then be investigated in a better way, and also more accurately represented in the model.

In this experimental study, the only indicator of the thermal effects of adsorption or desorption has been the temperature at various points in the carbon beds using thermocouples. A problem with this method is that the information of heat transfer is limited to the temperature at discrete points in the beds, thus limiting the information available. Another problem is the fact that the random packing of the carbon pellets causes an uncertainty of whether the the thermocouples are measuring the temperature in the gas phase or in direct contact with the solid phase. If considerable differences in temperature between the gas and solid phases exist, this method can potentially be inaccurate for the purpose of providing data for calibration of the thermal aspects of the model. The model suggests that such gradients are not significant (as shown in appendix E.1), but the experimental behaviour is unknown. Calorimetry could be a suitable complementary analysis method in order to better analyse and understand the thermal effects in the activated carbon during adsorption and desorption. In such a method, the heat flows to and from a suitable amount of activated carbon could be recorded over time during loading with n-butane and subsequent purge.

6.2 Isotherm parameter fitting

Isotherm data was given for temperatures of 25 and 100 °C. At normal conditions of purging without heating, the operating temperature of the experimental canister is always lower than 25 °C during purging (depending on the ambient temperature), and approaches values near 100 ° C only in the extremes of the loading case (as seen in Figure 5.2). This motivates the use of the parameter set obtained with the 25 °C-isotherm data, for the input of equation (3.6) in the model. However, it must be noted that the 25 °C-isotherm data set was given for pressures below one atmosphere (to a maximum pressure of 0.6 atm). This gives reason to question the accuracy of the chosen parameter set at atmospheric pressure. This potential issue aside, looking at the results in Table 5.1 it can be noted that the mean deviation of the modelled equilibrium loading from the experimental data at 25 °C and 100 °C is less than one percent of the limiting loading W_0, suggesting that the fit is good.

Another issue one may consider regarding the validity of the isotherm model is the case

where $\frac{W}{W_0} \to 0$, as mentioned in section 3.3. For a large enough extent of purge one may expect the coverage of n-butane on the carbon to approach zero. The results seem to indicate that the Dubinin-Astakhov isotherm works well with the LDF model for the durations of purge considered here, looking at Figure 5.5e. The potential weakness of the model for the extreme cases of coverage could perhaps have been more clearly seen if experiments with heating were performed, since the coverage in such a case can potentially approach near-zero values as suggested by the results in Figure 5.7c.

6.3 Validation and calibration of the model

Calibration with experimental data was attempted for the unknown parameters k_L in equation (3.6) and the enthalpy of formation of occupied active sites. As can be seen in Figure 5.5, the model is able to produce results that in some respects resemble the experimentally observed behaviour of the canister during purge. Regarding flow characteristics, the pressure drop modelling approach produces results in good agreement with the measured data as is shown in Figure 5.4, suggesting that the model predicts the flow through the canister satisfactory.

Considering the simulated and measured transient profiles of mass change given in Figure 5.5e, the results are similar with the largest differences in behaviour observed in the beginning of the purge event. The mass change can be argued to be one of the most important model outputs, since the performance of the canister is ultimately determined by the mass of fuel vapours that can be captured and removed during its operation. The agreement between the simulated and experimentally measured temperature profiles is not as good however, generally with the greatest similarities in the starting minutes of the purge event and at the inlets of the carbon beds. As seen in Figures 5.5a-d, there is an inertia in the experimental temperature profiles during purge that is not captured well by the model, suggesting that there are elements of the thermal aspects of the model that need improvement. Such elements could be for example the thermal properties of the carbon beds, although they were specified according to material data provided by the manufacturer. The fact that the simulated mass change due to desorption is in better agreement with the experimental data than the simulated temperatures can perhaps partially be attributed to the choice of weighting coefficients for the calibration procedure, as mentioned in section 4.2.3.

Figure 5.6 shows significant differences between the predicted transient temperature behaviour over the radius compared to the experimental behaviour observed. As shown in Figure 5.10, the heat transfer in the radial direction in the model appears to be more limited by the thermal conductivity of the carbon bed than the heat transfer on the external boundary (which is reasonable considering equation (3.15) for radial heat transfer depends only on λ_s). One may consider treating the thermal properties of the carbon bed as calibration parameters, but care must be taken to satisfy the experimental heat balance (which requires more data than provided

by the present experimental method) and to not calibrate physical parameters with nonphysical values. It is also possible that the description of radial heat transfer through only equation (3.15) is too simple, and that a more advanced model including for example dispersion effects (although not investigated in this project) is required to capture the radial effects well. The same can be said for the axial thermal effects.

However, caution must be exercised when comparing the simulated and experimental results, since the quality of the model calibration itself is questionable due to the lack of essential experimental data. The initial coverage in the purging case was somewhat arbitrarily assumed with an average value throughout the whole carbon bed length which was based on some initial simulations. It is likely that this did not represent the conditions in the experiments in an accurate manner. It is possible to specify an axial profile of coverage as an initial condition in the model, but no such data was available. The initial condition of coverage of butane on the carbon is important in the simulations since it affects the initial state relative to the equilibrium, and consequently affects the resulting mass change rate and temperature profiles in the canister. Thus, the settings for k_L, the enthalpy of formation and the initial coverage are not independent. This could be treated in a better way by more thoroughly investigating the degree of loading of the canister as discussed in section 6.1. Additionally, the enthalpy change due to desorption affects the rate of desorption via the temperature, and the temperature change is affected by the rate of reaction as well. The chosen method for calibration is therefore complicated by the coupled behaviour of of the associated parameters.

Another issue related to the specification of the initial coverage is the presence of possible gradients of coverage in the radial direction. The radial temperature gradients during loading and purging as shown for example in Figure 5.3 suggest that the carbon bed temperature is nonuniform over the radius, and therefore the radial profile of coverage can be expected to be nonuniform to some extent as well after the canister is loaded. Such information is likely not straightforward to obtain experimentally, and the options for such specifications in GT-SUITE are limited.

Furthermore, the enthalpy of formation should be calibrated to ensure that the heat balances in the experiments and simulated cases are consistent with each other. For in-depth studies of the efficiency of heat addition during purge, such consistency is likely essential. However, the present experimental method only allowed the transient temperature profiles to be compared with the simulated results. This issue can perhaps be resolved with smaller scale calorimetry experiments as mentioned previously, where the heat flow to or from a bed of carbon during the adsorption or desorption event is recorded. The enthalpy of formation in a representative model could then be calibrated to ensure that the simulated heat balance integrated over time is consistent with results from calorimetry experiments.

6.4 Purge air heating

Simulations were performed in which the purge flow was heated at each carbon bed inlet. The results are in line with the expected behaviour of the canister in response to heat input during purge, in that the mass of n-butane that can be purged and the rate at which this occurs are increased as shown in Figure 5.7. Therefore the model seems to produce physical results regarding purge heating. A reduction in the extra purged mass for each increment of total heat input is observed in Figure 5.7a, with the largest possible purged mass likely limited to the mass of n-butane present in the canister from the start. With a given requirement for efficiency of heat input with respect to the increase in purged mass, it is possible that there exists a limit in the amount of heat supplied beyond which the efficiency will be too poor to be viable. Comparing the profiles of mass change as in Figure 5.7b, the rate of change of mass will approach near-zero values with time, indicating that heating should be stopped after a certain time of purge depending on the criterion of efficiency.

In the context of heated purge, the resulting temperature of the flow can be large depending on the flow rate and heat input. This can also limit the possibilities for heating, with respect to the ability of the canister housing and carbon bed material to handle high temperatures. In the extreme case, the flammability of n-butane in air should also be considered.

In Figure 5.8 it is shown that as the total amount of heat supplied is shifted towards the inlet of the second carbon bed, the total purged mass is reduced. Considering that a uniform profile of coverage has been assumed throughout the bed length in the simulated cases, this result makes physical sense since half the carbon volume does not come in contact with hot air when all heat is supplied at the second bed. In such a case, it seems advantageous to supply all heat as early on as possible, which is also indicated by the difference in purged mass observed between cases 5 and 20, both having a total heat input of 80 W. It is possible that a different result could be obtained if a nonuniform coverage profile was specified, as is likely the case after the loading experiments carried out in this study. A heavier loading on the side where the n-butane enters the canister may motivate stronger heating close to it, if heat losses in the system are significant. No such data is available however, which motivates further experimental study.

It is crucial to note that the proposed canister model was validated against experimental data only under conditions where no heating of the purge air was applied. Under such conditions, the model produces physical results to some degree as compared to the measurements. However, since experiments with heated purge air could not be performed according to plan, it is uncertain if the behaviour of the model is sufficiently accurate under heated conditions. This is a severe limitation that must be kept in mind when using the model to predict the canister behaviour as a response to various heating conditions. Further experimental work is needed to provide experimental data with which the model can be validated under heated conditions. Furthermore,

the proposed model should not be regarded as a tool for simulating heating of real canisters to any meaningful accuracy, but rather as a tool for investigating possible effects of varying different parameters in relation to purge heating of carbon beds loaded with fuel vapours.

6.5 Assumptions regarding mass and heat transfer

Simplifications were made where intraparticle pore diffusion was neglected, along with the assumption in the LDF model that no intraparticle temperature gradients exist. The theoretical influences of these phenomena can be diagnosed by applying the Weisz-Prater and Anderson criteria. For the importance of internal pore diffusion, the Weisz-Prater parameter compares the observed reaction rate to the diffusion rate as

$$N_{W-P} = \frac{r_{obs} R_p^2}{C_s D_{eff}}$$

where r_{obs} is the observed reaction rate, R_p is the particle radius, C_s is the surface concentration on the particle and D_{eff} is an effective pore diffusivity of the adsorbate in the carbon in this case [39]. As a guideline, if $N_{W-P} \leq 0.3$ intraparticle pore diffusion limitations on the overall reaction rate can be assumed negligible, and intraparticle diffusion limitations are significant for $N_{W-P} > 0.3$. For intraparticle temperature gradients, the Anderson criterion is as follows:

$$\frac{|\Delta H| r_{obs} R_p^2}{T_s \lambda_s} < 0.75 \frac{R T_s}{E_r}$$

where E_r is the activation energy of the associated reaction. If the condition is fulfilled, intraparticle temperature gradients can be assumed negligible.

The numerical evaluations of the above criteria can be found in appendix C. The Weisz-Prater parameter is approximated for the conditions of purge in the present study to $N_{W-P} \approx 3$, indicating that intraparticle diffusion may limit the overall rate of the adsorption or desorption process. As for the Anderson criterion, the left hand side is estimated to $2 \cdot 10^{-4}$ and the right hand side to 0.06, suggesting that the criterion is fulfilled with approximately two orders of magnitude. This is an indication that the assumption of negligible intraparticle temperature gradients may be valid under the conditions considered.

This rough analysis indicates that an investigation regarding the influence of incorporating pore diffusion in the model can be of interest, while intraparticle heat transfer modelling can be regarded as superfluous in comparison. Modelling options for pore diffusion are available through the `SurfaceReactions`-template in GT-SUITE, although these were not explored in this thesis project.[7] The importance of intraparticle pore diffusion limitations could also be

[7] The ODE-solver for chemical reactions that must be used when modelling pore diffusion is not compatible with the ExhaustATDevice2D-object, making the concepts of 2D-modelling and pore diffusion modelling incompatible in GT-SUITE.

investigated experimentally by performing loading and purging experiments on different sets of carbon particles with different particle sizes.

6.6 Comparison of 1D and 2D simulations

Considering Figure 5.6, it is evident that the simulated radial temperatures deviate from the corresponding measured data. Under the assumption that temperature effects in the canister are of importance and considering that the results indicate a poor description of these by the model, one may question whether the 2D resolution applied in this study provides a meaningful increase to the accuracy of the model compared to the 1D case. From Figure 5.9 it can be concluded that the effect of simulating in 2D grows more important as the carbon bed diameter increases. To motivate the increase in CPU-time associated with the larger number of discrete volumes, it is important that the 2D model predicts the measurements well. Since the model was calibrated in the 2D configuration, the simulated temperatures of the 2D case were more in line with the experimental data than for the 1D case. However, it is not possible at this time to determine which one of the 1D and 2D setups that gives the best agreement with experimental data at large diameters, since such experimental data is unavailable. At the diameter of 70 mm corresponding to the experimental conditions of this study, the 1D and 2D cases perform equally well with respect to the simulated purged mass.

6.7 GT-SUITE as the choice of software

The advantage of using GT-SUITE to simulate the canister is the ease with which the model can be connected to other models in a larger system, in the extreme case allowing transient simulations of an entire vehicle system. As mentioned in section 3.4.1, GT-SUITE is inherently a 1D-modelling software with only a limited set of options for modelling in multiple dimensions. Thus, if a deeper understanding of flow, heat and mass transfer inside the canister is desirable, a review of the selection of methods and software may be in order. 3D CFD software such as Fluent or STAR-CCM+ are viable options with implementation of user-defined functions to model adsorption and heat transfer. For more intricate geometries such as real canisters, it is likely necessary to use 3D CFD software instead. For modelling of flow in smaller packed bed geometries, a CFD model based on the emerging Lattice Boltzmann methods could be interesting. However, detailed simulation of a randomly packed bed consisting of a large number of particles is still a very computationally demanding task, and geometry simplifications are necessary in any full-scale modelling application.

Chapter 7

Conclusions

A simulation model of a simplified canister capable of simulating radial heat transfer effects and heating of the purge flow was developed, validated with experimental data and tested in a parameter study. Thus the objectives of the thesis project were fulfilled. The simulated results produced by the model vary in accuracy with respect to the measured data. The Dubinin-Astakhov isotherm model was well fitted to isotherm data of n-butane adsorption on the carbon, and the flow characteristics in terms of pressure drop were well described by the model. The simulated canister mass change during the purge event agrees well with measurements, while the transient temperature profiles observed at various points in the axial and radial directions of the canister generally differ from the measured temperatures.

The experimental methods used in this study were found to be lacking for the purpose of providing data with which the model could be calibrated and configured. It is therefore uncertain if the canister model is well calibrated for different conditions and the reliability of the model is questionable.

The model can simulate heated purge for several different configurations of heat input to the canister. Although experimental data for validation is unavailable, the results from the simulated cases of purge heating agree with the expected behaviour of the canister in such cases. Heating becomes less efficient over time during purge and as more heat is supplied, and such effects can be roughly investigated with the use of the developed model.

The influence of simulating in 2D grows more important as the diameter of the canister is increased. For the canister diameter considered in this study, the 2D and 1D simulations can be regarded as equivalent with respect to the canister mass change, which is the most relevant result. Whether the 2D modelling provides increased accuracy relative to 1D modelling for different diameters remains unknown as such experimental data is unavailable.

Chapter 8

Recommendations for future work

The inadequacies of the experimental methods used in this study with respect to model calibration were discussed. As a remedy, future additions to the experimental method are likely necessary for the construction of a well calibrated model. Such additions can be for example evaluation of the concentration of n-butane in the carbon beds over time, and more thorough measurements of the heat flows to and from the canister to ensure consistency of the experimental and simulated heat balances.

Further experimental work is needed to validate the simulated canister behaviour as a response to heat input to the purge flow, as well as to validate the importance of radial heat transfer modelling with varying carbon bed diameters.

Pore diffusion modelling can be interesting as an addition to the canister model, as such limitations were revealed to potentially be of importance. Additional experiments with varying carbon particle sizes can also be of interest to investigate the effect of intraparticle diffusion limitations on the rate of desorption, and to validate the modelling of such effects.

Furthermore, it may be necessary in the future to review the choice of CFD modelling methods and software depending on the resolution and information desired from the model. For simulations with geometries closer to those of canisters mounted on vehicles, 3D CFD methods and software are likely needed.

Bibliography

[1] R. E. Hester, R. M. Harrison, and R. G. Derwent. "Volatile Organic Compounds in the Atmosphere". In: *Volatile Organic Compounds in the Atmosphere*. Ed. by R.E. Hester and Harrison R.M. 1st ed. Vol. 4. 4. Cambridge: The Royal Society of Chemistry, 1995. Chap. 1, pp. 1–16. ISBN: 978-1-84755-231-0. DOI: 10.1039/9781847552310-00001.

[2] Tingting Yue et al. "Characteristics of volatile organic compounds (VOCs) from the evaporative emissions of modern passenger cars". In: *Atmospheric Environment* (2017). ISSN: 18732844. DOI: 10.1016/j.atmosenv.2016.12.008.

[3] Philip J. Johnson, David J. Setsuda, and Roger S. Williams. "Activated Carbon for Automotive Applications". In: *Carbon Materials for Advanced Technologies*. Ed. by Timothy D. Burchell. 1st ed. Oxford: Elsevier, 1999. Chap. 8, pp. 235–268. ISBN: 9780080426839. DOI: 10.1016/B978-008042683-9/50010-8.

[4] Huan Liu et al. "VOC from Vehicular Evaporation Emissions: Status and Control Strategy". In: *Environmental Science and Technology* 49.24 (2015), pp. 14424–14431. DOI: 10.1021/acs.est.5b04064.

[5] P. J. Clarke et al. *An Adsorption-Regeneration Approach to the Problem of Evaporative Control*. Tech. rep. Warrendale, PA: Society of Automotive Engineers, 1967. DOI: 10.4271/670127.

[6] Uwe Mohr. "Activated carbon canisters for automobiles". In: *Filtration & Separation* 34.10 (Dec. 1997), pp. 1016–1018. DOI: 10.1016/S0015-1882(97)87275-8.

[7] Kazunari Sato and Noriyuki Kobayashi. "Adsorption and Desorption Simulation of Carbon Canister Using n-Butane as Model Compound of Gasoline". In: *Journal of the Japan Petroleum Institute* 54.3 (2011), pp. 136–145. DOI: 10.1627/jpi.54.136.

[8] In Kwang Yoo, Devesh Upadhyay, and Giorgio Rizzoni. *A Control-Oriented Carbon Canister Model*. Tech. rep. Warrendale, PA: Society of Automotive Engineers, 1999. DOI: 10.4271/1999-01-1103.

[9] Chongzhi Zhong et al. *The Influence on Working Performance of the Canister Cavity Design*. Tech. rep. Warrendale, PA: Society of Automotive Engineers, 2017. DOI: 10.4271/2017-01-1081.

[10] Philip J. Johnson, James R. Jamrog, and George A. Lavoie. *Activated Carbon Canister Performance During Diurnal Cycles: An Experimental and Modeling Evaluation*. Tech. rep. Warrendale, PA: Society of Automotive Engineers, 1997. DOI: 10.4271/971651.

[11] Freda Fung and Bob Maxwell. "Onboard Refueling Vapor Recovery: Evaluation of the ORVR Program in the United States". Washington DC, 2011.

[12] Werner Dabelstein et al. *Automotive Fuels*. Ullmann's Encyclopedia of Industrial Chemistry. 2007. DOI: 10.1002/14356007.a16_719.

[13] George A. Lavoie, Philip J. Johnson, and Jeffrey F. Hood. *Carbon Canister Modeling for Evaporative Emissions: Adsorption and Thermal Effects*. Tech. rep. Warrendale, PA: Society of Automotive Engineers, 1996. DOI: 10.4271/961210.

[14] Xingyan Bai et al. *Modeling and Simulation of N-butane Adsorption/Desorption in a Carbon Canister*. Tech. rep. Warrendale, PA: Society of Automotive Engineers, 2004. DOI: 10.4271/2004-01-1680.

[15] Ronald S. Joyce et al. *Activated Carbon for Effective Control of Evaporative Losses*. Tech. rep. Warrendale, PA: Society of Automotive Engineers, 1969. DOI: 10.4271/690086.

[16] P Bishop Robert and G Berg Peter. *Vapor Canister Heater for Evaporative Emissions Systems*. Tech. rep. Warrendale PA: Society of Automotive Engineers, 1987. DOI: 10.4271/870123. URL: https://doi.org/10.4271/870123.

[17] Alan Pittel and Ann Weimer. *High Vacuum Purge and Vapor Canister Performance*. Tech. rep. Warrendale, PA: Society of Automotive Engineers, 2004. DOI: 10.4271/2004-01-1435.

[18] Erik Möller. *Modelling and Simulation of an Activated Carbon Canister*. Tech. rep. Göteborg: Chalmers University of Technology, 2016.

[19] J.D. Seader, E.J. Henley, and D.K. Roper. *Separation Process Principles*. 3rd ed. Hoboken, NJ: John Wiley & Sons, 2010, p. 569. ISBN: 9780470481837.

[20] W. J. Thomas and B. Crittenden. "Fundamentals of adsorption equilibria". In: *Adsorption Technology & Design*. Oxford: Butterworth-Heinemann, 1998. Chap. 3, pp. 32–33. ISBN: 9780750619592.

[21] Peter Atkins, Julio de Paula, and Ronald Friedman. *Physical Chemistry: Quanta, Matter, and Change*. 2nd ed. Oxford, UK: Oxford University Press, 2014, pp. 914, 922. ISBN: 9780199609819.

[22] W. J. Thomas and B. Crittenden. "Rates of adsorption of gases and vapours by porous media". In: *Adsorption Technology & Design*. Oxford: Butterworth-Heinemann, 1998. Chap. 4, p. 66. ISBN: 9780750619592.

[23] S Sircar and D. V. Cao. "Heat of Adsorption". In: *Chemical Engineering & Technology* 25.10 (2002), pp. 945–948. DOI: 10.1002/1521-4125(20021008)25:10<945::AID-CEAT945>3.0.CO;2-F.

[24] E. Fiani, L. Perier-Cambry, and G. Thomas. "Non-isothermal modelling of hydrocarbon adsorption on a granulated active carbon". In: *Journal of Thermal Analysis and Calorimetry* 60.2 (2000), pp. 557–570. DOI: 10.1023/A:1010147005169.

[25] S. G. Chen and R. T. Yang. "Theoretical Basis for the Potential Theory Adsorption Isotherms. The Dubinin-Radushkevich and Dubinin-Astakhov Equations". In: *Langmuir* 10.11 (1994), pp. 4244–4249. DOI: 10.1021/la00023a054.

[26] P. S. Liu and G.F. Chen. "Chapter 1 - General Introduction to Porous Materials". In: *Porous Materials*. Ed. by P. S. Liu and G.F. Chen. 1st ed. Oxford, UK: Elsevier, 2014. Chap. 1, p. 1. ISBN: 978-0-12-407788-1. DOI: 10.1016/B978-0-12-407788-1.00001-0.

[27] H. Burnham Allport. *Activated carbon*. Web page of AccessScience. Retrieved 2018-02-16. Last updated 2017. 2017. DOI: 10.1036/1097-8542.009300. URL: https://doi.org/10.1036/1097-8542.009300.

[28] Harry Marsh and Francisco Rodríguez-Reinoso. "Activated Carbon (Origins)". In: *Activated Carbon*. Oxford: Elsevier Science Ltd, 2006. Chap. 2, pp. 27, 30, 48. ISBN: 9780080444635. DOI: 10.1016/B978-0-08-044463-5.50016-9.

[29] S. Sircar and J. R. Hufton. "Why Does the Linear Driving Force Model for Adsorption Kinetics Work?" In: *Adsorption* 6.2 (2000), pp. 137–147. DOI: 10.1023/A:1008965317983.

[30] N. D. Hutson and R. T. Yang. "Theoretical Basis for the Dubinin-Radushkevitch (D-R) Adsorption Isotherm Equation". In: *Adsorption* 3.3 (1997), pp. 189–195. DOI: 10.1007/BF01650130.

[31] Nicholas P. Cheremisinoff. "Vapor Pressure". In: *Pollution Control Handbook for Oil and Gas Engineering*. Ed. by Nicholas P. Cheremisinoff. Hoboken, NJ: John Wiley & Sons, 2016, pp. 1308–1309. ISBN: 978-1-5231-1032-2.

[32] P.J. Linstrom and W.G. Mallard. *NIST Chemistry WebBook, NIST Standard Reference Database Number 69*. Ed. by P.J. Linstrom and W.G. Mallard. Gaithersburg, MD: National Institute of Standards and Technology, 2017. DOI: 10.18434/T4D303. URL: http://webbook.nist.gov/cgi/cbook.cgi?ID=C106978&Mask=4&Type=ANTOINE&Plot=on.

[33] Gamma Technologies LLC. *GT-SUITE V2017 Flow Theory Manual*. 2017.

[34] Gamma Technologies LLC. *GT-SUITE V2017 Aftertreatment Manual*. 2017.

[35] Martin J. Rhodes. "Fluid Flow Through a Packed Bed of Particles". In: *Introduction to Particle Technology*. Ed. by Martin J. Rhodes. 2nd ed. Chichester, England: Wiley, 2008. Chap. 6, pp. 155–156. ISBN: 9780470727119.

[36] S. Mostafa Ghiaasiaan. "Analogy Among Momentum, Heat, and Mass Transfer". In: *Convective Heat and Mass Transfer*. New York, NY: Cambridge University Press, 2011. Chap. 9, pp. 259, 267. ISBN: 978-1-139-11101-0.

[37] R. Byron Bird, Warren E. Stewart, and Edwin N. Lightfoot. *Transport Phenomena*. 2nd ed. New York, NY: Wiley, 2002. ISBN: 0-471-41077-2.

[38] L Smith et al. *EVAP System Fluid-Dynamics and Chemistry Modelling for EMS Purge Control Development and Optimization.* Tech. rep. Suresnes: Société des Ingénieurs de l'Automobile, 2015.

[39] M. Albert Vannice. "Acquisition and Evaluation of Reaction Rate Data". In: *Kinetics of catalytic reactions.* Boston, MA.: Springer, 2005. Chap. 4, pp. 61–65. ISBN: 978-0-387-25972-7.

Appendix A

Experimental canister test rig

In Figure A.1 a detailed schematic of the experimental canister is given. Table A.1 provides a detailed description of the placement of thermocouples in the carbon beds.

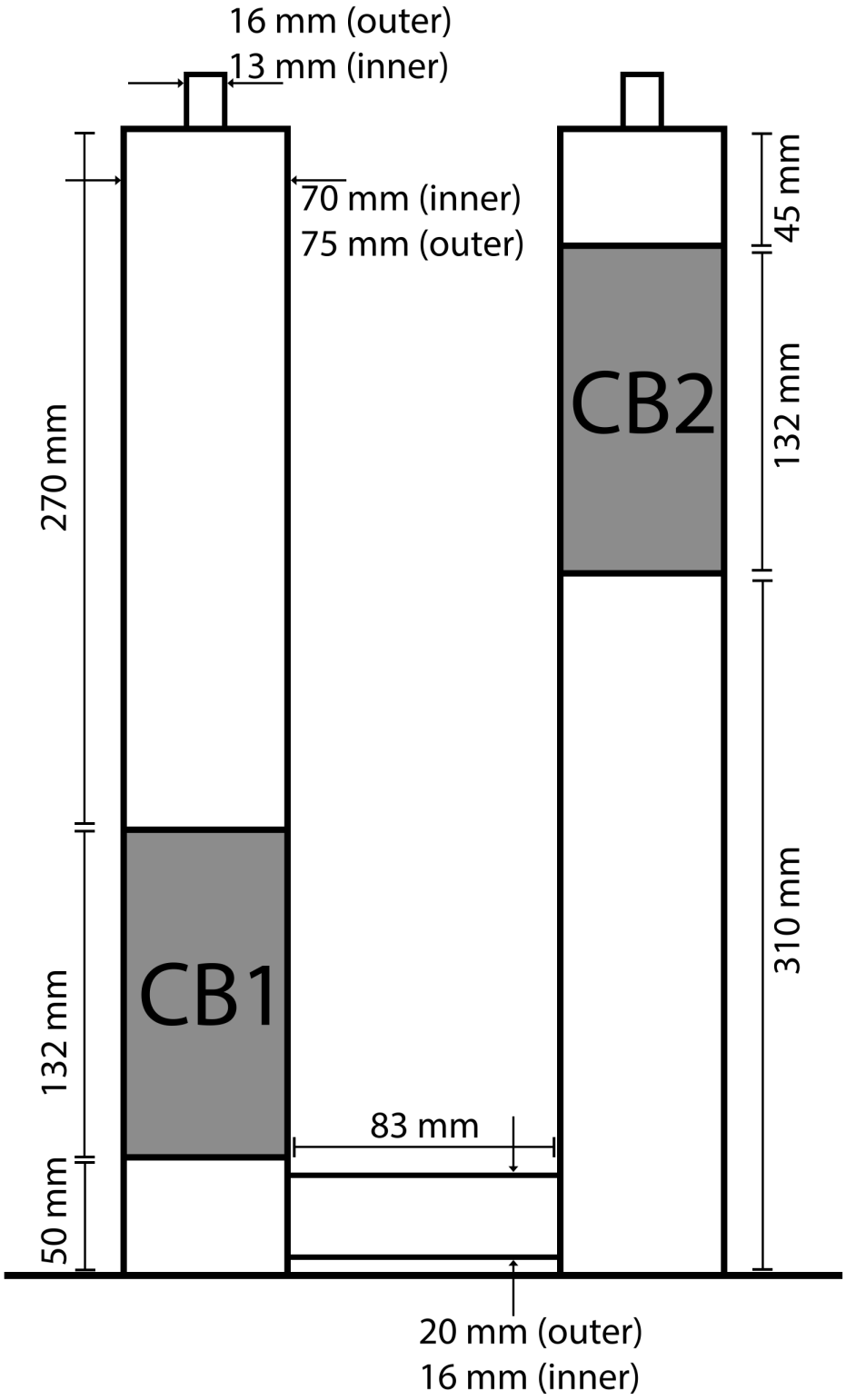

Figure A.1: Detailed schematic of the experimental canister. All measurements are approximate.

Table A.1: Positions of the thermocouples inserted into the carbon beds of the experimental test rig. The axial position is given with the inlet plates of the purging case as the reference for each bed. Both carbon beds are approximately 132 mm of length and have inner radii of 35 mm. All measurements are approximate.

Label	**Carbon bed**	**Axial position (mm)**	**Radial position from center (mm)**
1	1	-5 (above inlet plate)	0
2	1	-5 (above inlet plate)	28
3	1	26.4	0
4	1	26.4	14
5	1	26.4	28
6	1	52.8	0
7	1	52.8	14
8	1	52.8	28
9	1	79.2	0
10	1	79.2	14
11	1	79.2	28
12	1	105.6	0
13	1	105.6	14
14	1	105.6	28
15	1	137 (below outlet plate)	0
16	1	137 (below outlet plate)	28
17	2	-5 (below inlet plate)	0
18	2	-5 (below inlet plate)	28
19	2	26.4	0
20	2	26.4	14
21	2	26.4	28
22	2	52.8	0
23	2	52.8	14
24	2	52.8	28
25	2	79.2	0
26	2	79.2	14
27	2	79.2	28
28	2	105.6	0
29	2	105.6	14
30	2	105.6	28
31	2	137 (above outlet plate)	0
32	2	137 (above outlet plate)	28

Appendix B

GT-SUITE model information

In this appendix, details of specifications for the GT-SUITE model can be found.

B.1 GT-SUITE model objects

In Table B.1 the objects that were included in the GT-SUITE simulation model are presented with descriptions of each object.

Table B.1: Objects used in the GT-SUITE simulation model.

Object	**Description**
EndFlowInlet	Takes settings for inlet boundary conditions
EndEnvironment	Takes settings for outlet boundary conditions
InletPipe	Round pipe part used for the inlet pipes to the carbon beds
FlowSplitGeneral-Heater	General flow volume used for heat input to the flow
nocond	Virtual orifice connections to the carbon beds
CarbonBed	Models the packed beds of carbon
FlowSplitGeneral	General flow volumes that the carbon beds must connect to
ConnectionBend	Models the T-pipe shape associated with the connection of the two columns of the experimental setup
FlowSplitGeneral-ConnectionExpansion	Models the pipe expansion/contraction of the pipe part associated with the connection between the columns
ConnectionPipe	The pipe part connecting the columns
OutletPipe	The pipe part at the outlet of the second carbon bed

Table B.2: Wall material specifications for the carbon beds and pipe parts in the GT-SUITE model.

Property	Value
Thickness	2.5 mm
Specific heat capacity	1800 J/kg,K
Thermal conductivity	0.1 W/m,K
Density	900 kg/m^3

B.2 Specifications in SurfaceReactions

The specifications for reactions in the `SurfaceReactions`-object are made in the following format:

$$Rate = [Preexp]T^a \exp\Big(-\frac{E_A}{RT}\Big)\theta(i)\{conc\}G(i)$$

where $Rate$ is the reaction rate, $[Preexp]$ is a pre-exponential factor, a is a temperature exponent, E_A is an activation energy, $\theta(i)$ is a coverage dependent expression, $\{conc\}$ is a concentration dependent expression and $G(i)$ is a general function. In order to express the rate according to equations (3.6) and (3.7) the following settings were made:

- $[Preexp] = [LDF\_k]$ (case parameter)
- $a = 0$
- $E_A = 0$
- $\{conc\} = 1$
- $\theta(i) = G(1) - A(2)$

where $G(1)$ represents the exponential term in equation (3.6) and $A(2)$ represents the fractional coverage species as defined under "Coverages". Explicitly, the general function $G(1)$ was entered as:

```
exp(-([R]*T*ln((if(T>272.66,(10^5)*10^(4.35576-1175.581/(-2.071+T)),(10^5)*
10^(3.85002-909.65/(-36.146+T))))/(P*max({C4H10},1e-8)/(P/([R]*T))))/[E])^[n])
```

Appendix C

The Weisz-Prater and Anderson criteria

For the evaluation of the Weisz-Prater criterion, the magnitude of the observed reaction rate at its maximum is taken from the results from a simulation of the purge event in GT-SUITE as 1 mol/m^3,s. The corresponding n-butane surface concentration is approximated from the same set of results with the gas phase concentration as 1.75 mol/m^3. The effective pore diffusivity is approximated with the following expression for the Knudsen diffusivity presented by Do and Do[a].

$$D_K = \frac{2r}{3}\sqrt{\frac{8RT}{\pi M}}$$

where D_K is the Knudsen diffusivity, r is the average micropore size, R is the universal gas constant, T is the temperature and M is the molar mass of the adsorbate. For their calculation of the Knudsen (pore) diffusivity in activated carbon, Do and Do used an average micropore size of 1 nm. For a temperature of 5 °C, a molar mass of $58.12 \cdot 10^{-3}$ kg/mol for n-butane and an assumed average micropore size of 1 nm, the Knudsen diffusivity evaluates to approximately $2 \cdot 10^{-7}$ m^2/s. For a particle radius of 1.075 mm, the Weisz-Prater parameter evaluates to approximately 3.

For the Anderson criterion, the enthalpy of reaction is taken equal to the adsorption enthalpy found by Fiani et al as 22 kJ/mol, and the activation energy for desorption is estimated in the same study to 30 kJ/mol[b]. The same reaction rate, temperature and particle radius as for the

[a] Do, D.D. and Do, H.D. "Surface diffusion of hydrocarbons in activated carbon: Comparison between constant molar flow, differential permeation and differential adsorption bed methods". In: *Adsorption* 7.3 (2001), pp. 189–209.

[b] Fiani E., Perier-Cambry L., Thomas G. "Non-isothermal modelling of hydrocarbon adsorption on a granulated active carbon". In: *Journal of Thermal Analysis and Calorimetry* 60.2 (2000), pp. 557-570.

Weisz-Prater criterion applies, and the activated carbon thermal conductivity is taken as 0.4 W/m,K as investigated by Jin et al.[c]. This gives a left hand side of $2 \cdot 10^{-4}$ and a right hand side of 0.06.

[c]Jin, Z. et al. "Comparison on thermal conductivity and permeability of granular and consolidated activated carbon for refrigeration". In: *Chinese Journal of Chemical Engineering* 21.6 (2013), pp. 676-682.

Appendix D

The previous and present canister models

In this study, the model development procedure and the resulting model were similar to the work performed in the thesis project by Möller in 2016 [18]. In this study however, there are some differences in choices regarding how to model certain aspects of the canister.

Probably the most important difference lies in whether the enthalpy of formation of occupied sites is treated as a calibration parameter or not. In the previous thesis work, the parameter was specified as -145 kJ/mol which corresponded to an isosteric enthalpy of adsorption of -20 kJ/mol added together with the enthalpy of formation for n-butane of -125 kJ/mol, both found in the literature [18]. The enthalpy of formation parameter in GT-SUITE was therefore specified based on physical quantities from the literature rather than calibrated. There was however no clear motivation presented for why this should be the case. Since the adsorption of n-butane on activated carbon is considered a physisorption process (see section 3.1) it should not undergo chemical change or chemical bonding, and consequently the justification for including the enthalpy of formation for n-butane is unclear. In another canister modelling study performed by Smith et al.[d] the parameter was calibrated, which motivates the adoption of the method in this study. This gives differences in the magnitudes of temperatures obtained between the studies.

Another difference is how the bed of activated carbon is modelled. In the study from 2016 it was modelled as a monolithic catalyst support with a washcoat inside square channels, whereas in the present study the bed of carbon is modelled to represent an actual packed bed of particles, with the intention of bringing more physical resemblance to experimental setup that is actually being modelled. Representing the carbon bed as a packed bed of particles via the "General

[d]Smith, L. et al. *EVAP System Fluid-Dynamics and Chemistry Modelling for EMS Purge Control Development and Optimization.* Suresnes: Société des Ingénieurs de l'Automobile, 2015.

geometry"-option presents an advantage in an increased level of flexibility regarding transport properties in the bed, with user-input options for the specific area and solid fraction as well as correlations for pressure drop, heat and mass transport. In the case where the carbon bed is modelled as a monolith with square channels, the options are limited to specifications for wall thickness and channel density, with common heat and mass transport correlations for channel flow pre-determined in the software. The difference in behaviour between two corresponding configurations in the two approaches during the simulations however is not significant. The simulated pressure drops at higher purge flow rates are underestimated in the previous as well as in the present model, indicating similar physical behaviour as a result of the two approaches. A slightly higher pressure drop is produced by the packed bed modelling approach compared to the channel geometry approach.

Additionally, there is a difference in the formulation of the Dubinin-Astakhov isotherm model. In the present study, an error in the previous formulation was corrected where the fraction inside the ln-term of the Dubinin-Astakhov model equation was previously written $\frac{p_s}{y_{n-butane}}$ where $y_{n-butane}$ was the molar fraction of n-butane, thus resulting in an error of units. New isotherm data was collected for the present study and the fitting procedure was done with the corrected fraction of pressures, resulting in a different parameter set. This does not affect the results regarding the description of adsorption equilibrium much except for new values of the isotherm parameters, but it gives improved physical consistency which is advantageous when debugging the model. As a consequence of the new parameter fitting, it was found that using a temperature-dependent saturation pressure gave a better fit to the isotherm data, as opposed to using a fixed saturation pressure which was done by Möller.

In the `SurfaceReactions`-template, the Diffusion setting was previously configured as "Obsolete". This means that a concentration gradient between the gas and solid phases is solved for [34]. However, the setting is regarded as an old and inefficient model setting that will eventually be removed.[e] The preferred options are either "Diffusion On", where the gradient of concentration of the reacting species is also solved for, or "Diffusion Off" where the concentration of the reacting species is assumed uniform from the gas to the surface of the solid phase. In this thesis project, the setting "Diffusion Off" was used in order to separate the effect of mass transfer between the Diffusion-setting and the k_L in equation (3.6). When switching between "Diffusion Off" and "Diffusion On" the results are similar with only small differences in the resulting temperatures and canister mass change profiles, indicating that the setting does not have an important effect on the final result.

In regards to the model performance, the present model can be said to perform with similar accuracy compared to the previous model. The behaviour of the temperature profiles during

[e] Jonathan Brown, Gamma Technologies, 2018-02-08. Personal communication.

purge show similarities in that the temperature rises more quickly from the minimum in the simulated cases compared to the measurements. The profiles of mass change during a purge event are also similar. This is an indication that the different approaches to certain elements of the canister model discussed above do not severely affect the final results produced.

Appendix E

Transient temperature profiles in the gas and solid

Figure E.1 shows the temperature variations in time in the fluid and solid phase at four different points in the carbon beds. As can be seen, the differences in temperature between the phases are not significant.

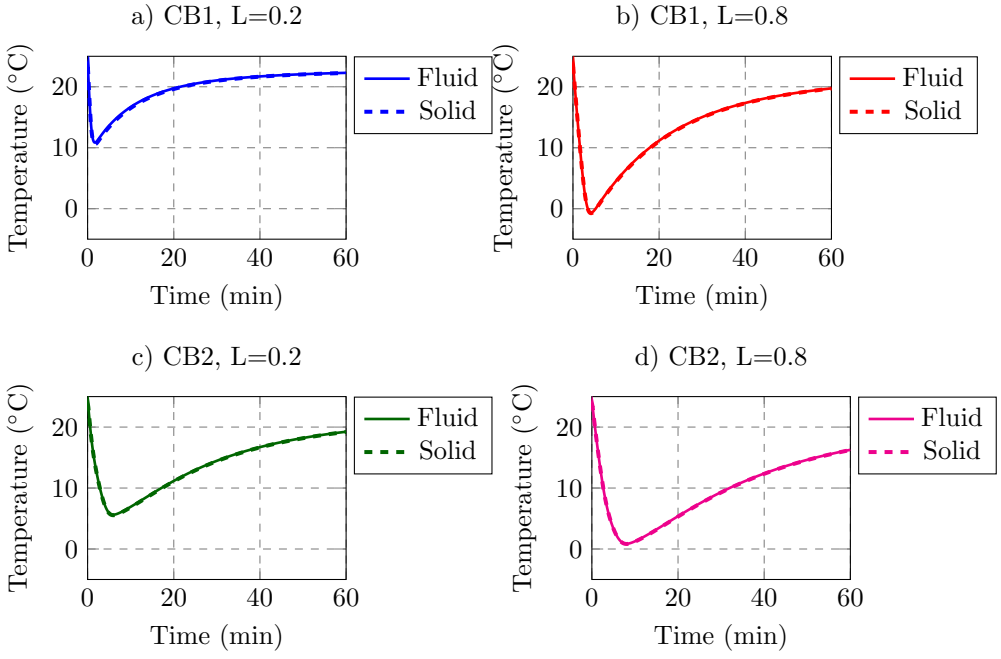

Figure E.1: Simulated temperatures in the fluid and solid phase, compared at the beginning (0.2) and end (0.8) along the axial direction of each carbon bed.